Assessment of Scientific Creative-Potential by Near-Infrared Spectroscopy Using Brain-Network Based Deep-Fuzzy Classifier

Sayantani Ghosh, *Graduate Student Member, IEEE,* Amit Konar, *Senior Member, IEEE,* and Atulya K. Nagar

***Abstract*—The work presents a novel approach to assess the scientific creative ability of subjects by analyzing their brain connectivity patterns through functional Near-Infrared Spectroscopy (fNIRS) during participation in an analogical reasoning test. The proposed method involves three key stages: i) construction of brain connectivity networks using Wavelet Transform Coherence (WTC), ii) abstraction and analysis of three node-based network features, and iii) classification of abstracted features into five degrees of creative potential by a novel Enhanced Graph Convolution Induced Type-2 Fuzzy Classifier (EGCIFC). The novelty of the classifier lies in: i) design of an enhanced graph convolution operation that encapsulates local and global structural information from the input graph, ii) use of the Smish activation function to improve performance, iii) inclusion of a one-dimensional spatial convolution layer for preserving relevant information within convolved embeddings, iv) design of a novel mapping function to mitigate uncertainty among the spatial convolved vectors in the type-2 fuzzy layer, and v) application of Takagi-Sugeno-Kang (TSK)-based fuzzy reasoning to reduce computational cost. Evaluation on three datasets, each comprising over 45 individuals from different scientific backgrounds, shows that EGCIFC improves classification accuracy by 2.25% over the nearest competitor and by 22.72% over the lowest-performing baseline. The proposed method also reduces computational cost by 7.46% and 54.7% compared to the nearest and worst competitors, respectively. Additionally, EGCIFC exhibits a standard deviation of ±0.72% in classification accuracy, reflecting its robustness. Hence, the proposed approach may prove effective for recruiting individuals with varying degrees of scientific creativity across different research sectors.**

***Index Terms*—fNIRS, creativity, brain network, Capsule GNN, deep fuzzy classifier**

I. Introduction

Scientific creativity [1], [2] refers to the ability to transcend conventional thinking and generate novel ideas that foster progress in science, technology, industry, and/or society. It acts as a driving force behind scientific breakthroughs that help expand the frontiers of human insight. There exists several cognitive factors that are responsible for shaping creative outcomes in scientific realm which include spatial reasoning [3], inductive learning [4], convergent thinking [5] and many others [6], [7]. In addition to the aforementioned cognitive factors, the ability to draw comparisons between two or more distinct concepts based on their structural and/or functional similarities, plays a crucial role in facilitating scientific creativity [8], [2], [9]. This ability, referred to as analogical reasoning, has shown to be responsible for several major discoveries and innovation in science. For instance, Niels Bohr drew an analogy between the structure of an atom and the solar system that laid the foundation for quantum mechanics. Similarly in biology, Louis Pasteur explained the working principle of antibodies through an analogy of a lock and key mechanism that helped in the development of vaccines. Likewise, René Descartes revolutionized mathematics by introducing the concept of coordinates by drawing similarities between geometry and algebra. Thus, analogical reasoning, as illustrated by the above examples, strongly influences the genesis of novel outcomes in scientific domain. The present work aims to assess the scientific creative skill of individuals from their analogical reasoning ability using functional Near-Infrared Spectroscopy (fNIRS).

The current research employs the Raven's Advanced Progressive Matrices (RAPM) [10] test to examine the scientific creative ability of individuals. In this test, individuals are required to identify patterns, relationships, and logical structures among abstract visual elements to determine a missing piece of a figure. This process thus mirrors analogical reasoning, where recognizing similarities and correspondences between different elements is essential for finding solutions. Although RAPM test is widely used to examine the fluid intelligence of subjects [11], which encompasses various logical reasoning abilities [12] such as deductive reasoning, analogical reasoning and the like, it primarily captures the analogical reasoning component more prominently [13], [14], [15], [16]. Moreover, research studies in [17], [18], [19] confirm the utilization of the aforesaid test for assessing scientific creative potential. Therefore, the use of the RAPM test constitutes an appropriate choice for the present study.

Existing literature [20], [21] on the RAPM test focuses on examining the cognitive strategies required to solve problems associated with such tests. In a different vein, Friedman et al. [22] utilized the Electroencephalography (EEG) technique for evaluating the cognitive load experienced by subjects during the Raven's test. Alternatively, a recent study by Xu et al. [23] employed an EEG based classification algorithm to distinguish between confused and non-confused mental states of subjects while solving the Raven's test. Other research [24], [25], [26] on the aforesaid test focuses on exploring the active brain regions involved during the problem solving process utilizing functional Magnetic Resonance Imaging (fMRI). In a similar context, Amin et al. [27] and Jawed et al. [28] independently employed EEG signal analysis to examine the active brain regions and the dominant frequency bands involved in the present cognitive task. On the contrary, Ociepka et al. [29] focused solely on examining the influence of different frequency bands of EEG signals on the Raven's problem solving

Sayantani Ghosh and Amit Konar are with the Artificial Intelligence Laboratory, Department of Electronics and Tele-Communication Engineering, Jadavpur University, Kolkata, India.

Atulya K. Nagar is with the Department of Mathematics and Computer Science, Liverpool Hope University, Liverpool, UK.

task. Additionally, Luo et al. [30] and Amin et al. [31] independently performed EEG based experiments to investigate the participation of different Event related Potentials (ERPs) while solving the Raven's test.

Unfortunately, studies exploring the relationship between a subject's creative potential and their brain connectivity during the RAPM task remain largely unexplored. This study aims to fill this void by examining the fNIRS based brain connectivity associated with analogical reasoning in RAPM tasks to assess the subject's creative potential. In a very recent study, Ghosh et al. [32] examined the creative ability of subjects during the Raven's test by utilizing EEG signal analysis. Though EEG is a widely used brain signal acquisition technique due to its high temporal resolution [33], [34], it is less effective at localizing neural activity due to volume conduction [35], which in turn leads to a reduction in spatial accuracy of recorded signals. On the contrary, fNIRS captures the changes in cerebral blood flow by providing moderately high spatial resolution, thereby enabling more reliable acquisition of brain activation patterns. Furthermore, advanced brain imaging techniques offering high spatial resolution like fMRI, are often impractical for experimental use due to its high price and limited accessibility. Thus, fNIRS provides a cost effective and computationally efficient alternative, making it a suitable modality for the present study.

The objective of the current research is to evaluate individual differences in creative ability through the RAPM task. The above evaluation is carried out in three phases. In the first phase, the fNIRS signals recorded from the scalp of participants engaged in the RAPM task are pre-processed and converted into a brain connectivity network using the Wavelet Transform Coherence (WTC) [36] method. In the second phase, three node based features are extracted from the acquired brain networks which include node strength (NS), node efficiency (NE) and node betweenness (NB) [37]. The rationale behind the feature extraction process is to examine the Brodmann Areas (BAs) of the brain that serve as primary controllers of the entire network during the processing of the RAPM task. In the third phase, the extracted features pertaining to each node is utilized to classify the creative ability of participants into five distinct levels: Extremely Creative Thinker (ECT), Superbly Creative Thinker (SCT), Fairly Creative Thinker (FCT), Mildly Creative Thinker (MCT) and Conventional Thinker (CVT).

The prime contribution of the present work involves the development of a classifier model that is specifically designed to handle the above classification problem. As the present work deals with brain connectivity networks, the classifier model is constructed on the framework of a Graph Convolution Network (GCN) [38], [39], a popular deep learning approach for classifying graph based data [40], [41]. A classical GCN model consists of two main modules. The first module abstracts the features form the input graph via graph convolution and pooling while the second module classifies the abstracted features using fully connected layers [39]. However, fNIRS signals collected from a given source are susceptible to fluctuations both within and across sessions due to parallel thoughts, extrinsic and/or intrinsic artifacts [42], [43] that introduces uncertainty within the abstracted features [44], [45], [46]. To combat the aforesaid issue, the present classifier architecture incorporates an Interval Type-2 Fuzzy (IT2F) layer within the GCN model.

In this paper, a novel classifier model, referred to as Enhanced Graph Convolution Induced Type-2 Fuzzy Classifier (EGCIFC) has been designed to classify the fNIRS signals of individuals into five distinct levels of creative potential (i.e., ECT, SCT, FCT, MCT and CVT). The original contributions of the EGCIFC model includes:

1) Formulation of an enhanced graph convolution operation, capable of capturing both local and global structural information from the input graph that enables the classifier to learn diverse patterns from the same graph.
2) Utilization of the Smish [47] activation function after the enhanced graph convolution operation, due its capability to generate non-zero responses for small negative inputs, in order to improve classification accuracy.
3) Introduction of a one-dimensional (1D) spatial convolution layer after the enhanced graph convolution, instead of pooling, to retain the most significant information within the convolved embeddings.
4) Design of a novel mapping function in the IT2F layer that captures the most promising region in the Footprint of Uncertainty (FOU) [48] in order to minimize the uncertainty among the spatially convolved vectors.
5) Employment of Takagi-Sugeno-Kang (TSK) [49]-based fuzzy reasoning for handling the present classification task in order to reduce computational cost by eliminating the additional need for defuzzification and type-reduction.

Performance analysis undertaken against the state-of-the-art (SOTA) algorithms demonstrates the proposed model's effectiveness in classifying the different degrees of creative potential. Comprehensive comparative studies, including ablation based analysis, further highlight the proficiency of the proposed approach. Additionally, statistical validation also confirms the model's efficacy in performing the classification task.

The rest of the paper is arranged as follows. Section II discusses the steps required to perform the present classification task. Section III delves into the formulation of the proposed classifier model. Section IV outlines the experimental paradigm and discusses the results of the cognitive experiment. Section V portrays the comparative studies conducted to demonstrate the efficacy of the proposed model, while Section VI provides the conclusions drawn from the paper.

II. Problem Formulation and Approach

This section presents a brief summary of the cognitive experiment undertaken for the present research. Fig. 1 represents the block diagram of the proposed experimental paradigm. The experiment begins by acquiring the brain signal of participants using the fNIRS device who have volunteered for the RAPM task. The RAPM task utilized for the current experiment consists of 4 sets of problems with variation in difficulty levels [11], [50]: 1) easy, 2) medium, 3) hard and 4) extremely hard. An exemplar problem used for the present experiment

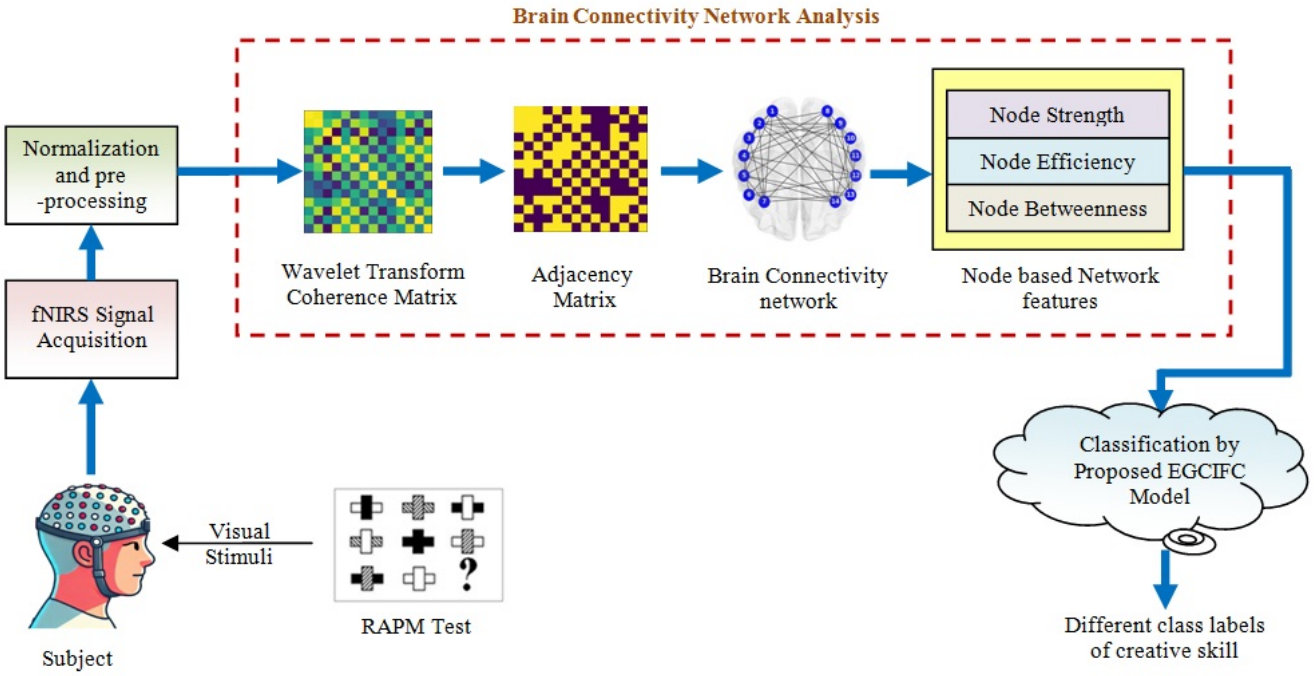

Fig. 1. Block diagram of the proposed experimental framework illustrating the main modules utilized for classifying different degrees of creative potential of subjects.

for medium difficulty level is portrayed in Fig. 2. Each difficulty level consists of 5 problems. A single session of the experiment pertaining to each difficulty level consists of 5 trials. The structure of the visual stimuli used for the current cognitive activity for a single session is depicted by Fig. 3. The stimulus begins with a fixation cross of 3 seconds followed by a time-frame of 15 seconds where the RAPM problem needs to be solved mentally by the participant. After this, a time-frame of 10 seconds is provided where the participant verbally informs the experimenter about the answer to the RAPM task. The aforesaid process is repeated for four more number of problems. Thus, for 10 experimental days and 5 sessions in a day, 5 problems/trial × 5 trials/session × 5 sessions/day × 10 days produces 1250 experimental instances corresponding to each participant.

After the brain signal acquisition phase is over, the signals are normalized, pre-processed and converted into a brain connectivity network using the WTC technique. The nodes in the aforesaid network represent the BAs corresponding to a given montage while the edges represent the connections between the nodes. Subsequently, three node based features (strength, efficiency and betweenness) are abstracted from the formulated brain networks and analyzed to identify the BAs acting as prime controllers for the present cognitive task. The abstracted nodal features from each experimental instance are utilized by the proposed EGCIFC model to categorize subjects into one of five grades of creative ability: 0) Non-Creative/Conventional Thinker (CVT), 1) Mildly Creative Thinker (MCT), 2) Fairly Creative Thinker (FCT), 3) Superbly Creative Thinker (SCT), and 4) Extremely Creative Thinker (ECT).

As mentioned above, the RAPM test includes 4 sets of problems, where each set comprises 5 problems. The problem sets have correspondence to grades 1 to 4. The test begins with grade 1 problem-set. A subject who is able to correctly answer at least 4 out of 5 questions (i.e., $\geq 80\%$) in the grade-1 problem set qualifies to attempt the grade-2 problem set. In general, a person appearing at grade j test-problems, will be qualified to appear at grade $j+1$ test-problems with the condition that he/she has to correctly answer at least 4 out of 5 questions of grade j problem-set, where j varies in [1, 3]. However, if a subject fails to answer at least 4 questions of a selected grade, he/she is considered to belong to the next lower grade. For example, a subject eligible to appear for grade-4 test, unfortunately answers ≤ 3 questions of grade-4 correctly, then he/she is declared to have a grade-3, i.e., Superbly Creative Thinker. It is obvious that a subject failing to win grade-1 test is declared to lie in grade-0, i.e., CVT.

It is important to note that the threshold for passing the screening test in a given category is subjective and so, in general, can take any value in [0, 100]%. A higher threshold obviously provides greater precision in determining a subject's highest creativity grade. In this study, the 80% threshold selected requires a subject to correctly answer at least 4 out of 5 questions. As the present setup does not allow any threshold between 80% and 100%, and the choice of 100% threshold is too restrictive, leaving the 80% threshold as the option for the current experimental setup.

Unfortunately, there are no standard scientific creativity validity indices, as appears in different problem-domains (e.g., cluster validity indices to test the quality of a new clustering algorithm). However, as discussed in Section I analogical reasoning acts as one of the fundamental modalities for assessing

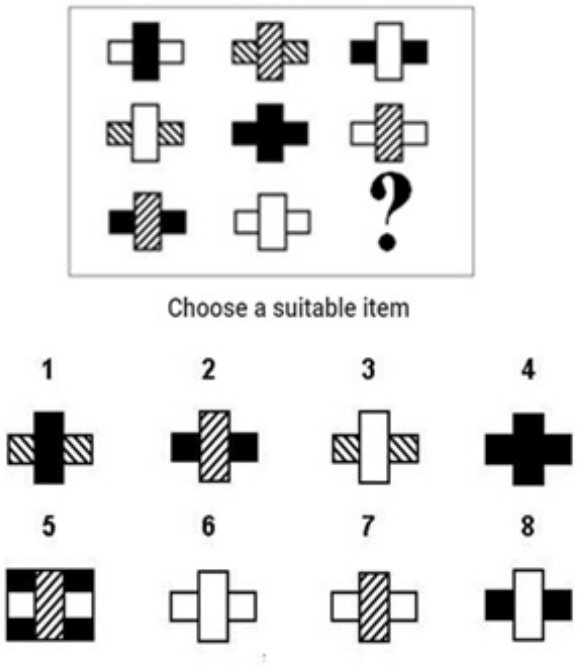

Fig. 2. An exemplar RAPM problem of medium difficulty level

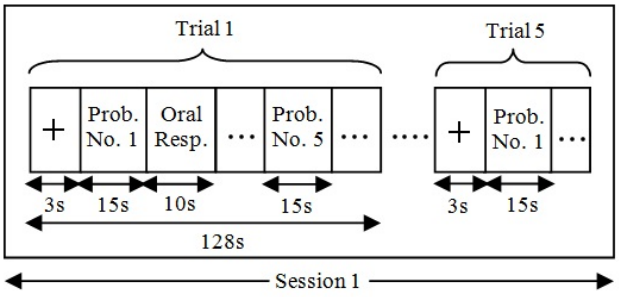

Fig. 3. Structure of visual stimuli used for the RAPM task for a given difficulty level pertaining to a single session

scientific creative ability. The rationale behind the proposed labels for scientific creativity is grounded in the assumption that a subject's ability to solve difficult analogical reasoning problems reflects a higher level of creative potential [51], [52], [53], [54]. The RAPM-based analogical reasoning task is supported by existing literature [17], [18], [19] as a valid approach for assessing scientific creativity. Therefore, assigning the label ECT to a subject, capable of correctly solving extremely hard problems, and assigning relatively lower grades SCT, FCT, and MCT for correctly answering problems of lower difficulty levels hence makes sense. Thus, the proposed labeling scheme has a logical basis in assigning a grade of creativity to distinct subjects based on their performance in RAPM test.

The main steps of the current experiment, as discussed above, are summarized in Algorithm A.I, provided in the Appendix [55], under Section A.I. The details of the aforementioned phases are discussed below.

A. EVALUATION OF NORMALIZED CEREBRAL OXYGEN EXCHANGE

The first step in analyzing the acquired raw fNIRS signals is to assess the net oxygen consumption in the brain's cortical region, quantified by the metric known as cerebral oxygen exchange (COE) [56], [57]. The steps required for computing the aforementioned metric are elaborated below.

The fNIRS data collected from the scalp of participants captures two key blood concentration measurements: oxy-hemoglobin (O_2Hb) and deoxy-hemoglobin (HHb), both expressed in mmol/L. Let $\Delta O_2Hb(t)$ and $\Delta HHb(t)$ represent the changes in concentrations of O_2Hb and HHb respectively, corresponding to a channel of the given montage at time t during an experimental instance. Since, $\Delta O_2Hb(t) > \Delta HHb(t)$, $\forall t$ [44], [45], [46] COE at any time t is evaluated by (1).

$$C_0 = \Delta O_2Hb(t) - \Delta HHb(t) \tag{1}$$

The normalized value of COE within the range [0,1] is computed by (2).

$$\hat{C}_0 = \frac{\Delta \mathrm{O_2Hb}(t) - \Delta \mathrm{HHb}(t)}{max(\Delta \mathrm{O_2Hb}(t)) - min(\Delta \mathrm{HHb}(t))} \tag{2}$$

where,$max(\Delta \mathrm{O_2Hb}(t))$ indicates the maximum value of $\Delta \mathrm{O_2Hb}(t)$ at time t while $min(\Delta \mathrm{HHb}(t))$ signifies the minimum value of $\Delta \mathrm{HHb}(t)$ at time t.

B. ELIMINATION OF DIFFERENT ARTIFACTS FROM RAW FNIRS SIGNALS

After normalizing the net oxygen consumption induced fNIRS signals, the next step involves eliminating various artifacts that may have been introduced into the raw signals during the acquisition stage. The artifacts affecting the fNIRS signals can be broadly classified into two categories [42], [43]: i) extrinsic artifacts and ii) intrinsic artifacts. Extrinsic artifacts originate from external factors unrelated to the subject's physiological state. Extrinsic artifacts can be of two types: a) Technical: these involve instrumental noise, which may result from variations in the equipment's sensitivity, calibration issues, or inconsistencies in optode placement on the scalp, leading to differences in signal detection across trials or participants, and b) Environmental: these refer to external conditions that can impact fNIRS signal readings, such as ambient light interference, temperature fluctuations, and other similar factors. Intrinsic artifacts in fNIRS signals are primarily physiological noises and fluctuations that disrupt the accurate measurement of cerebral hemodynamics. These include cardiac pulsation, respiration, blood pressure variations, Mayer waves (low-frequency blood pressure oscillations linked to vasomotor activity that impact blood oxygenation), and motion artifacts (disturbances in fNIRS signals caused by physical movement).

A comprehensive signal processing approach is implemented to eliminate the aforementioned artifacts from the fNIRS signal. Initially, the normalized values of COE for all channels are filtered using a Chebyshev band-pass filter of order 6, with a passband range set at 0.01 to 3.5 Hz. The selection of the Chebyshev band-pass filter is made

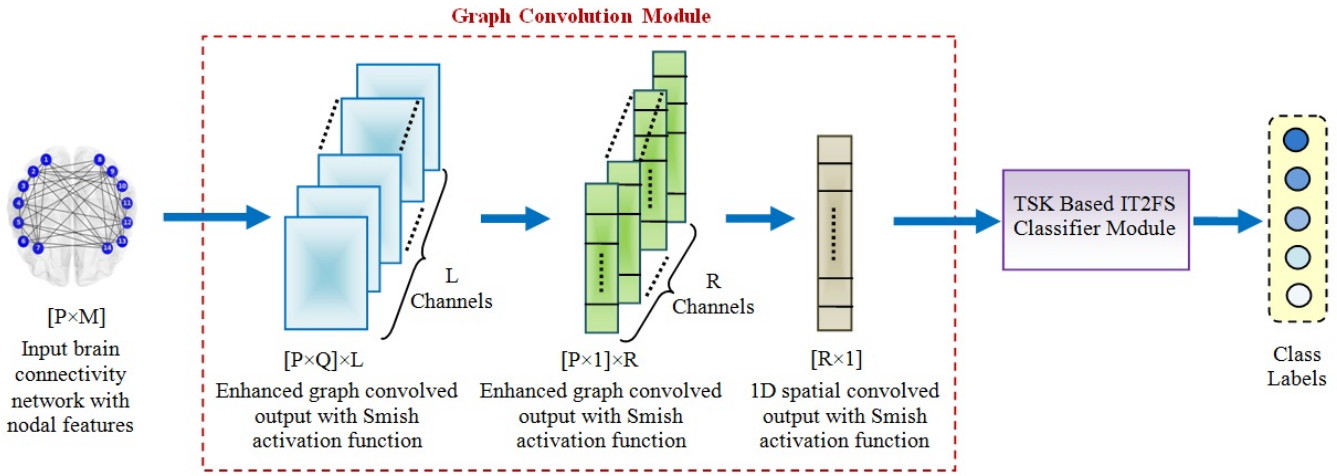

Fig. 4. Overview of the architectural framework of the proposed Enhanced Graph Convolution Induced Fuzzy Classifier (EGCIFC) model

due to its ability to achieve a sharper roll-off, enhancing the separation of frequency components while maintaining a manageable level of ripple within the pass-band [58]. A detailed analysis justifying the optimal choice of the above filter is provided in the Appendix [55] under Section A.II due to space economy. Following the filtering stage, Independent Component Analysis (ICA) is performed on the filtered signals using the FastICA algorithm [59]. The number of independent components is set equal to the number of measurement channels (here, 14). Artifact components are identified using a kurtosis-based method [60], [61], where kurtosis is defined as a measure of the "peakedness" of the probability distribution of the time course of each independent component. Independent components whose probability distributions sharply peaked at the center (i.e., kurtosis ¿ 10) are considered artifact-dominated and are removed. Next, the denoised signals are reconstructed by back-projecting the remaining components.

C. FORMATION OF BRAIN CONNECTIVITY NETWORKS

The filtered fNIRS signals are processed using wavelet transform coherence (WTC) to explore their behavior across time and frequency domains. This approach quantifies the cross-correlation between two time-series signals over varying time and frequency scales [36], [62]. The WTC between two fNIRS channels, X and Y, at the time instance n (denoted as X_n and Y_n) is mathematically defined by (3).

$$V_n(s) = \frac{|\langle s^{-1} V_n^{XY}(s)\rangle|^2}{|\langle s^{-1} V_n^{X}(s)\rangle|^2 \, |\langle s^{-1} V_n^{Y}(s)\rangle|^2} \tag{3}$$

where, s represents the wavelet scale, n denotes the time instance, $V_n^X(s)$ and $V_n^Y(s)$ indicates the continuous wavelet transform of X_n and Y_n respectively, $|\cdot|$ denotes the absolute value and $\langle\cdot\rangle$ represents the smoothing operation [62]. For the present application, the Daubechies wavelet [63] is utilized as the mother wavelet for evaluating the WTC among the pair of FNIRS channels.

Using the operation in (3), a $P \times P$ matrix is generated, representing the wavelet coherence between pairs of fNIRS channels. These coherence values are subsequently employed to build an undirected, weighted connectivity network using the following approach in (4).

$$a_{ij} = \begin{cases} V_{ij}, & \text{if } V_{ij} \geq \xi \\ 0, & \text{otherwise} \end{cases} \tag{4}$$

where, a_{ij} denotes the adjacency matrix values of the connectivity network, V_{ij} indicates the wavelet coherence values while ξ indicates a predefined threshold. The predefined threshold is chosen in such a way that all classes of networks have the same number of edges, ensuring a fair comparison among them [64].

D. FEATURE ABSTRACTION OF THE CONNECTIVITY NETWORKS

To identify the hub regions of the brain that govern the entire network, the brain connectivity networks derived from the WTC technique needs to be analyzed through various network topological features. This analysis is carried out by extracting three key features: node strength (NS), node efficiency (NE), and node betweenness (BC) [37].

The extracted features are ultimately categorized into five distinct classes using the EGCIFC classifier, with its detailed architecture explained in Section III.

E. Classification Metrics utilized to analyze the performance of the EGCIFC

The performance metrics utilized to prove the efficacy of the proposed EGCIFC algorithm in comparison to conventional approaches include: classification accuracy (CA), F1-score, True Positive Rate (TPR), False Positive Rate (FPR) and run-time complexity. The mathematical expressions for CA, F1-score, TPR and FPR are defined by (5), (6), (7), (8) respectively.

$$CA = \frac{T_P + T_N}{T_P + T_N + F_P + F_N} \tag{5}$$

$$F1 = \frac{2T_P}{2T_P + F_P + F_N} \tag{6}$$

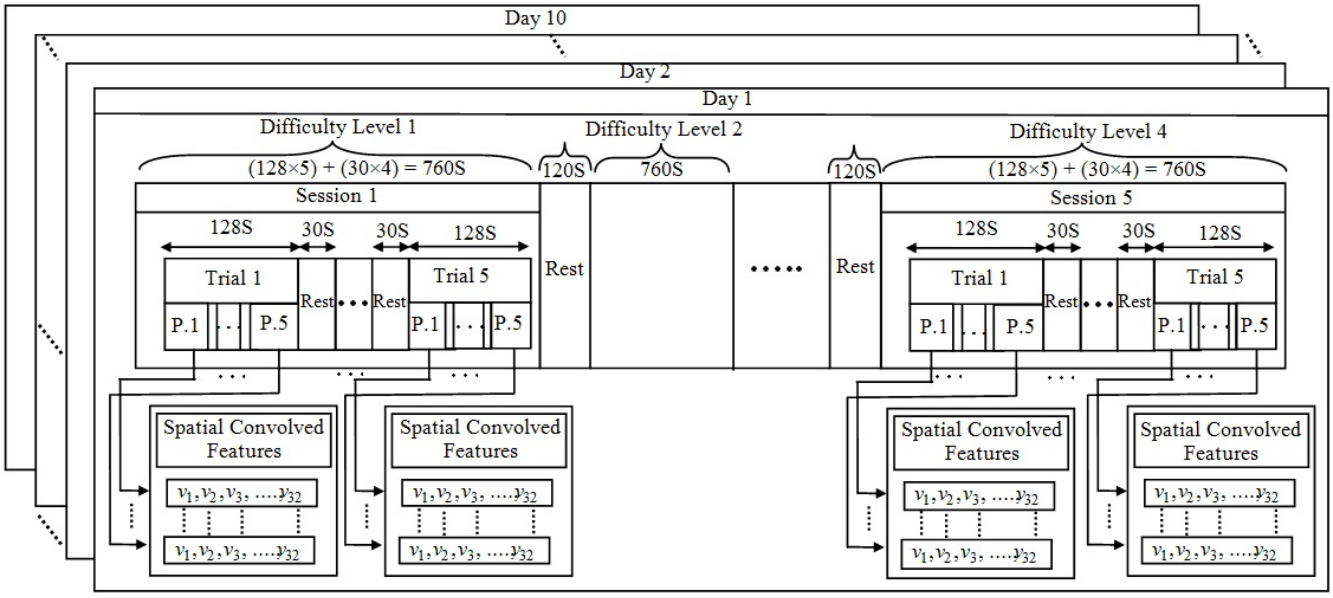

Fig. 5. The spatial convolved features obtained from each problem of a trial in a session pertaining to a given difficulty level for every experimental participant

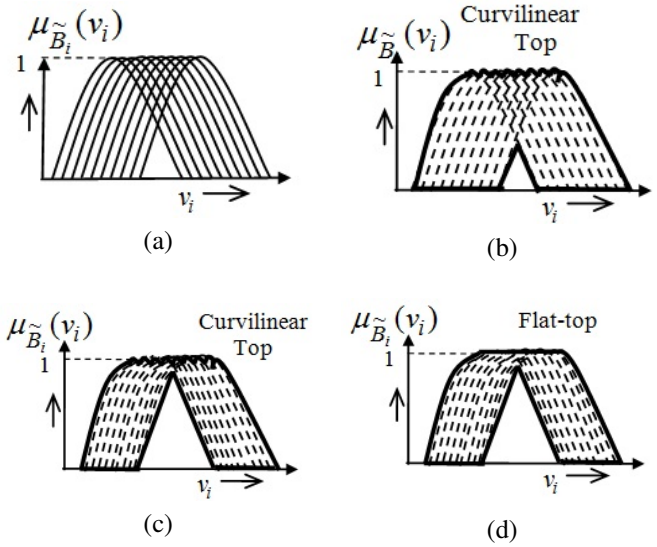

Fig. 6. Construction of IT2FS with refined FOU: (a) Type-1 MFs for 10 days, (b) Curvilinear-top based IT2FS formulated by taking union of Type-1 MFs, (c) Curvilinear-top based IT2FS with refined FOU, (d) Flat-top approximated IT2FS.

$$TPR = \frac{T_P}{T_P + F_N} \tag{7}$$

$$FPR = \frac{F_P}{F_P + T_N} \tag{8}$$

where, T_P, T_N, F_P and F_N denotes the number of true positives, true negatives, false positives and false negatives respectively.

III. ARCHITECTURE OF THE PROPOSED ENHANCED GRAPH CONVOLUTION INDUCED TYPE-2 FUZZY CLASSIFIER

This section provides a detailed explanation of the proposed EGCIFC model, whose architecture is depicted in Fig. 4. The description and functions of each layer of the proposed classifier model are discussed below.

A. FIRST ENHANCED GRAPH CONVOLUTION LAYER WITH SMISH ACTIVATION FUNCTION

The first layer of the proposed classifier includes the employment of an enhanced graph convolution operation and Smish activation function. The elaboration of the above operations is provided below.

1) ENHANCED GRAPH CONVOLUTION: A given input graph $G \in \mathbb{R}^{P \times M}$ is transformed into its graph embeddings using the traditional graph convolution operation [38] which can be mathematically expressed by (9).

$$Z_j^{k+1} = \sigma(\sum_i \tilde{D}^{-1/2} \tilde{A} \tilde{D}^{-1/2} Z_i^k W_{ij}^k) \tag{9}$$

where, $Z^k \in \mathbb{R}^{P \times M}$ represents the input graph in the k^{th} layer of size $P \times M$ and $Z^0 = G$. $W_{ij}^k \in \mathbb{R}^{M \times M'}$ signifies the matrix of trainable weights of size $M \times M'$ while $\sigma(\cdot)$ indicates an activation function. $\tilde{A} = A + I$ denotes the adjacency matrix A consisting of self-loops, $I \in \mathbb{R}^{P \times P}$ represents the identity matrix of size $P \times P$, and $\tilde{D}$ signifies the degree matrix of $\tilde{A}$.

However, the traditional graph convolution operation relies solely on the adjacency matrix A, which captures only the local structure of the graph. As a result, it aggregates information exclusively from the immediate neighbors of a node, neglecting the influence of distant neighbors. This reduces the classifier's performance, as it cannot effectively learn diverse

patterns within the same graph from multiple perspectives due to its confinement to local structural information.

To address the aforementioned limitation, the present work modifies the adjacency matrix to incorporate both local and global structural information of the graph using (10).

$$E = exp(A) \approx I + A + \frac{A^2}{2!} + \frac{A^3}{3!} \tag{10}$$

The computation in (10) describes the series expansion of the exponential operation applied to A, approximated up to the third order. In (10), the matrix I incorporates self-loops, A captures the local structural information of the graph, and the higher-order terms of A represent the global structural information of the graph, extending up to the third-distant neighbor. It may be noted that the truncation of the expansion in (10) to the third order is determined by the random search algorithm [65] discussed in Section IV.

Thus, the computation in (9) is now modified using the new adjacency matrix E in (11), ensuring that the convolved features from the input graph capture both local and global structural information.

$$Z_j^{k+1} = \sigma(\sum_i \tilde{D}^{-1/2} E \tilde{D}^{-1/2} Z_i^k W_{ij}^k) \tag{11}$$

where, E denotes the modified adjacency matrix and $\tilde{D}$ now represents the degree matrix of E. The convolution operation in (11), hereafter referred to as the enhanced graph convolution, thus enables the classifier to learn diverse patterns from a single graph, ultimately improving its performance.

2) EMPLOYMENT OF SMISH ACTIVATION FUNCTION: A new activation function referred to as Smish [47] is utilized for the current work instead of traditional ones. The mathematical equation for this function is denoted by (12).

$$\sigma(x) = Smish(x) = x \cdot tanh(ln(1 + \rho(x))) \tag{12}$$

where, $\rho(x)$ denotes the sigmoid activation function. The motivation behind the utilization of Smish involves the following points: i) it has enhanced regularization capability as it maintains negative output regularization and partial sparsity, thereby preventing over-fitting, ii) it ensures smooth and stable gradient flow through the application of the $tanh$ operator on a logarithmic transformation and iii) it has shown to be highly robust across various hyper-parameters [47], ensuring consistent performance for different experimental settings.

B. SECOND ENHANCED GRAPH CONVOLUTION LAYER WITH SMISH ACTIVATION FUNCTION

An additional enhanced graph convolution with Smish activation function is performed upon the graph convolved output from the first layer using (11) and (12). This additional operation ensures that the higher level features are abstracted from the previously convolved output so that classifier model can effectively capture intricate patterns from the input data. The output of the present operation yields $J \in \mathbb{R}^{(P\times 1)\times R}$ where $P \times 1$ denotes the dimension of each convolved vector and R represents the number of channels (see Fig. 4).

C. 1D SPATIAL CONVOLUTION LAYER

The objective of the present layer involves reducing the dimension of the graph convolved features as well as retaining the most significant feature information that will be utilized for classification. The traditional GCNs usually rely on pooling operations to accomplish the aforesaid objective [39]. However, pooling comes with two main limitations. First, unlike convolution, pooling does not utilize kernel based operations having weights that are learned during training, thereby failing to capture relevant features from the input data. Second, popular pooling techniques either ignore finer details by only retaining the most prominent features (max-pooling) or over-smoothes the feature set by blending all information (mean-pooling).

Thus, to overcome these limitations, the current work utilizes a 1D spatial convolution on the second graph convolved output. The 1D spatial convolution operation is denoted by (13).

$$h_j = \sigma((g_i * w_{ij}) + \beta_j) \tag{13}$$

where, $h_j \in \mathbb{R}^{1\times 1}$ represent the 1D spatial convolved output, $g_i \in \mathbb{R}^{P\times 1}$ denotes the second graph convolved output for a single channel of size $P \times 1$, $\sigma(\cdot)$ signifies the Smish activation function, $w_{ij} \in \mathbb{R}^{P\times 1}$ indicates the weight matrix of size $P \times 1$, β_j is the bias term and "$*$" represents the spatial convolution operator. The operation in (13) is repeated for all the R channels which thereby produce R number of scalar values. These R scalars are stacked into an $R \times 1$ dimensional vector which represents the output of present spatial convolution layer to be used later for classification. Thus, the $R \times 1$ vector contains the most relevant abstracted features from J using spatial convolution that will guide the classifier to distinguish the desired class labels.

D. TSK INDUCED INTERVAL TYPE-2 FUZZY LAYER

The 1D spatial convolution layer generates a feature vector of size $R \times 1$ (where R=32) for every RAPM problem as denoted by Fig. 5. To handle the uncertainty arising in these convolved feature vectors due to sessional variations, a TSK-induced Interval Type-2 Fuzzy Set (IT2FS) classifier is employed. The aforementioned approach is detailed below.

1) FORMULATION OF ANTECEDENT PART OF IT2FS CLASSIFIER: Let, $v_1, v_2, ..., v_N$ be N features obtained at the output of the 1D spatial convolution layer. Let $\tilde{B}_i = [\overline{\mu}_{\tilde{B}_i}(v_i), \underline{\mu}_{\tilde{B}_i}(v_i)]$, $i = 1$ to N, represent an IT2FS with Upper Membership Function (UMF) = $\overline{\mu}_{\tilde{B}_i}(v_i)$ and Lower Membership Function (LMF) = $\underline{\mu}_{\tilde{B}_i}(v_i)$. The construction of $\tilde{B}_i$ is accomplished by the following steps. First, the within-session variations of measurements of feature i is represented by a Gaussian type-1 Membership Function (MF) [66], [67] with mean m_i and variance σ_i^2. The Gaussian type-1 MFs acquired from 10 experimental days (i.e., representing within-session variations) is depicted by Fig. 6(a). Next, the across-session variations for feature i is the union of the MFs defined by the within-session variations. In IT2FS nomenclature, the UMF of feature i is obtained by taking the maximum of the

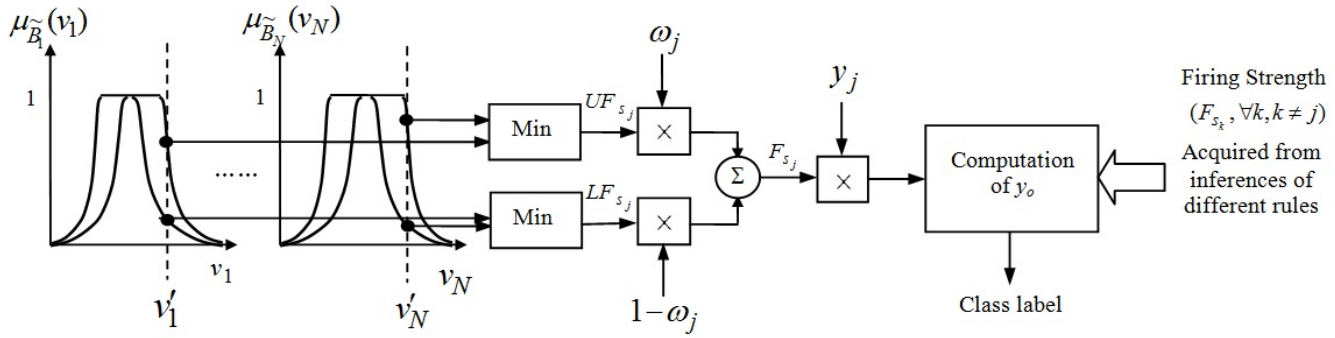

Fig. 7. Design of the proposed TSK induced Interval Type-2 fuzzy classifier

Gaussian MFs representing the within-session variations of the same feature. Similarly, the LMF is obtained by taking the minimum of the within-session variations of the i^{th} feature. Expressions (14) and (15) are obtained following the above formulation.

$$UMF = \overline{\mu}_{\tilde{B}_i}(v_i) = \underset{j=1}{\overset{N}{\text{Max}}}(\mu_{B_j}(v_i)) \tag{14}$$

$$LMF = \underline{\mu}_{\tilde{B}_i}(v_i) = \underset{j=1}{\overset{N}{\text{Min}}}(\mu_{B_j}(v_i)) \tag{15}$$

where, $\mu_{B_j}(v_i)$ denotes the type-1 Gaussian MF of the j^{th} session for feature v_i. The above IT2FS construction is represented by Fig. 6(b).

In IT2FS nomenclature, the measure of uncertainty is often expressed by the area under the Footprint of Uncertainty (FOU) [48]. The FOU is measured by the area lying between the UMF and the LMF. One approach to reduce the uncertainty in IT2FS is to shift up the LMF towards UMF [46], [68] thereby causing a reduction in the area under the FOU. This paper employs dilation [67], [69], [70] of the LMF for its possible lifting towards the UMF by a heuristically chosen transformation given by (16).

$$LMF_{new} = \underline{\mu}_{\tilde{B}_i'}(v_i) = \overline{\mu}_{\tilde{B}_i}(v_i) \times (\underline{\mu}_{\tilde{B}_i}(v_i))^{\underline{\mu}_{\tilde{B}_i}(v_i)} \tag{16}$$

The transformation (16) transforms the LMF $\underline{\mu}_{\tilde{B}_i}(v_i)$ into $\underline{\mu}_{\tilde{B}_i'}(v_i)$ to level up the LMF (see Fig. 6(c)). Theorem 1 provides a formal proof to indicate that $\underline{\mu}_{\tilde{B}_i'}(v_i) \geq \underline{\mu}_{\tilde{B}_i}(v_i)$, for all v_i, but $\underline{\mu}_{\tilde{B}_i'}(v_i)$ never crosses $\overline{\mu}_{\tilde{B}_i}(v_i)$. It is important to mention that the UMF of the newly adjusted FOU remains unchanged i.e., $\overline{\mu}_{\tilde{B}_i'}(v_i) = \overline{\mu}_{\tilde{B}_i}(v_i)$.

Theorem 1: *The transformation* (16) *elevates* $\underline{\mu}_{\tilde{B}_i'}(v_i)$ *so as to satisfy* $\underline{\mu}_{\tilde{B}_i'}(v_i) \geq \underline{\mu}_{\tilde{B}_i}(v_i)$, *maintaining* $\underline{\mu}_{\tilde{B}_i'}(v_i) \leq \overline{\mu}_{\tilde{B}_i}(v_i)$ *for all* v_i.

The proof of Theorem 1 is presented under Section A.III of the Appendix [55] to avoid loss in continuity of the context.

The updated IT2FS given by $\tilde{B}_i'$ appears to have a non-convexity due to its curvilinear top that has been acquired by considering maximum of the 10 type-1 MFs (shown in Fig. 6(c)). Thus, to retain the convexity of the designed type-2 fuzzy sets, a flat-top approximation is employed upon the acquired IT2FS. Such an approximation is achieved by connecting the peaks of the individual type-1 MFs with a straight line of zero slope [44], [45], [46]. The final flat-top approximated IT2FS is portrayed in Fig. 6(d).

2) FORMULATION OF CLASSIFIER RULE: The proposed TSK model utilizes Type-2 fuzzy rule where the j^{th} rule is given by,
If v_1 is $\tilde{B}_{1,j}'$, v_2 is $\tilde{B}_{2,j}'$,.....,v_N is $\tilde{B}_{N,j}'$, Then
$y_j = \sum_{i=1}^{N} \phi_{i,j} \times v_i + \lambda_j$.
Here, y_j represents the power of the signal pertaining to a given montage architecture which is utilized to categorize different class labels. The coefficients $\phi_{i,j}$ and λ_j are determined utilizing the classical least min-square approach [71].

E. IMPLEMENTATION OF THE TSK-BASED IT2FS CLASSIFIER

The design of the proposed fuzzy induced classifier is illustrated in Fig. 7. Let the measurements points be denoted as $v_1 = v_1^{'}$, $v_2 = v_2^{'}$, ..., $v_N = v_N^{'}$. The upper firing strength (UF_s) and lower firing strength (LF_s) for the j^{th} rule is computed utilizing (17) and (18) respectively.

$$UF_{s_j} = min[\overline{\mu}_{\tilde{B}_1'}(v_1^{'}), \overline{\mu}_{\tilde{B}_2'}(v_2^{'}), ..., \overline{\mu}_{\tilde{B}_N'}(v_N^{'})] \tag{17}$$

$$LF_{s_j} = min[\underline{\mu}_{\tilde{B}_1'}(v_1^{'}), \underline{\mu}_{\tilde{B}_2'}(v_2^{'}), ..., \underline{\mu}_{\tilde{B}_N'}(v_N^{'})] \tag{18}$$

After this, the firing strength (F_s) pertaining to rule j is computed using (19).

$$F_{s_j} = \omega_j \cdot UF_{s_j} + (1 - \omega_j) \cdot LF_{s_j} \tag{19}$$

where, ω_j denotes a weight lying in $[0, 1]$ and is determined by the random search algorithm. The final output of the TSK induced type-2 fuzzy classifier is evaluated using (20).

$$y_0 = \frac{\sum_{\forall j} F_{s_j} \times y_j}{\sum_{\forall j} F_{s_j}} \tag{20}$$

In order to categorize the five desired class labels from the computation of y_0, the interval $[0, y_0^{max}]$ is divided into five non-overlapping regions. So, for five regions, four different region boundaries are required which include η_1, η_2, η_3 and

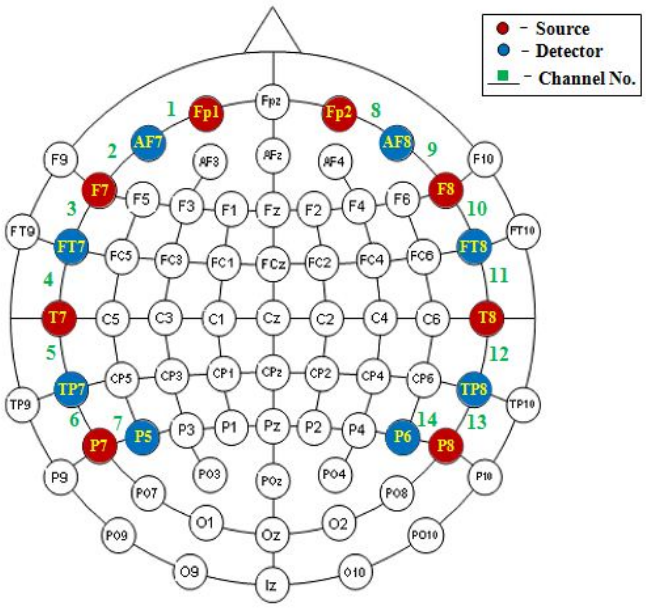

Fig. 8. Architecture of the montage designed for the RAPM task

η_4. The aforementioned region boundaries are determined by the random search algorithm satisfying: $y_0^{max} > \eta_4 > \eta_3 > \eta_2 > \eta_1 > 0$.

IV. EXPERIMENTS AND RESULTS

A. FNIRS DATA ACQUISITION

The current experimental framework was carried out in the Artificial Intelligence Laboratory (AI Lab) of Jadavpur University situated in Kolkata, India. The hemodynamic response of participants during the RAPM task was acquired using the whole-brain fNIRS device (NIRScout TM) developed by NIRx Medical Technologies, LLC. This device comprises 8 infrared sources and 8 detectors and operates at 7.81 Hz sampling rate. The source-detector pairs referred to as optodes were places on the scalp of participants according to the 10-10 international optode placement system. Although the NIRScout device provided 64 channels, only 14 were selected for analysis. This selection was based on the nearest-neighbor source-detector configuration as well as the anatomical relevance of the regions to cognitive functions of interest. The selected channels primarily overlay the prefrontal and parietal lobes, which are well-documented in the literature [24], [32], [72] as key regions involved in analogical reasoning and higher-order cognitive tasks, justifying their inclusion in the present cognitive experiment. The montage architecture used in the experiment is shown in Fig. 8.

B. PARTICIPANTS

A priori power analysis was conducted using the G*Power 3.1.9.4 software [73] to determine the required sample size for the present cognitive experiment. The analysis indicated that a total sample size of 144 participants was needed to achieve a statistical power of 0.9, using Analysis of Variance (ANOVA) with a medium effect size (f = 0.3) and an error probability $\alpha = 0.05$. To account for potential dropouts or errors during the experiment, three datasets were prepared with total 149 participants. The three datasets are as follows:
i) West Bengal Creativity Dataset (WBCDS) [74]: This dataset comprises 52 participants (23 males and 29 females), including 18 from engineering, 12 from mathematics, and 22 from general science backgrounds, aged between 18 and 36 years.
ii) Southwest Indian Creativity Dataset (SWICDS) [75]: This dataset comprises 47 participants (24 males and 23 females), including 14 from engineering, 16 from mathematics, and 17 from general science backgrounds, aged between 23 and 45 years.
iii) North Indian Creativity Dataset (NICDS) [76]: This dataset comprises 50 participants (29 males and 21 females), including 16 from engineering, 16 from mathematics, and 18 from general science backgrounds, aged between 21 and 40 years.

All participants included in the experiment had normal or corrected-to-normal vision with no prior history of neuropsychiatric or motor disorders. Moreover, the participants must have attended undergraduate courses in science/engineering. This restriction was made mandatory, as the present experiment focused on the assessment of scientific creativity [77], [78]. Additionally, participants were selected to ensure diversity in age groups, genders, cultures, education levels, and regional backgrounds, in order to minimize potential demographic and/or cognitive biases.

The data of two participants (I21 and I44) from WBCDS were excluded from the study due to data inconsistencies, and the data of one participant from NICDS (I26) was excluded because the subject was unable to complete the experiment due to sudden illness.

Fig. 9 portrays the experimental setup using one representative subject solely for demonstration purposes, while the experiments were conducted on 52, 47, and 50 subjects for the WBCDS, SWICDS, and NICDS datasets, respectively. The experiment strictly adhered to ethical guidelines and safety protocols, in accordance with the Declaration of Helsinki (1970), as revised in 2004 [79]. Ethical approval for the study was obtained from the Ethics Committee of Jadavpur University, and the corresponding report is provided in [80].

C. COGNITIVE INSIGHTS INTO BRAIN NETWORK FEATURE ANALYSIS

The brain connectivity networks of participants belonging to each class label have been acquired using the WTC technique as discussed in Section II. The different connectivity networks pertaining to the five class labels obtained from a single experimental instance are depicted in Fig. 10. The nodes in each network represent the BAs covered by the channels in the montage shown in Fig. 8, while the edges signify the connections among the BAs. However, in order to identify the active engagement of the BAs for the current cognitive task, three node based features are abstracted form the acquired brain networks. The analysis of these features is presented in detail below.
(a) **NS Analysis**: Fig. 11(a) illustrates the radar plot of NS values for five classes of subjects. It is observed from this

Fig. 9. Experimental setup for the RAPM task

figure that NS values for nodes 1, 8 and 14 are high for participant I27 who belongs to the ECT class. Moreover, the same nodes exhibit quite high NS values for participants I11, I09 and I32 belonging to SCT, FCT and MCT classes respectively. Such an observation signifies that bilateral anterior prefrontal cortex (BA 10) pertaining to nodes 1 and 8 and right posterior supramarginal gyrus (BA 40) pertaining to node 14 possess high degree for participants who could correctly solve the RAPM task. Additionally, the NS values are also high for nodes 2 and 9 for the participant belonging to ECT class. However, these values start declining slowly for the participants from the SCT to MCT class. The former observation implies that the bilateral region of dorsolateral prefrontal cortex (BA 46) pertaining to nodes 2 and 9 also possess high degree for the RAPM task. The later observation indicates that BA 46 controls the level of difficulty of the RAPM task. In other words, higher the NS value for nodes pertaining to BA 46, higher is the difficulty level of the given task. It is also important to note that the NS values of node 4 for subject I09 and node 6 for subject I32 exhibit moderately high values. Thus, a further analysis of additional node based features is necessary to derive concrete conclusions about the most engaged nodes in the brain network of creative individuals.

(b) **NE Analysis**: Fig. 11(b) illustrates the radar plot of NE values for the same set of subjects discussed earlier. Notably, for a subject in the ECT class, elevated NE values are evident over the bilateral part of anterior prefrontal cortex (nodes 1 and 8) and right posterior supramarginal gyrus (node 14). Similarly, the NE values for subjects in the SCT, FCT and MCT classes also show heightened NE values for the aforesaid regions. Additionally, the bilateral part of dorsolateral prefrontal cortex (nodes 2 and 9) shows high NE values, with a clear decreasing trend from the ECT to MCT classes. Furthermore, the NE analysis indicates that the highlighted BAs for creative class individuals do not exhibit significant activation in a person who could not solve the RAPM task (i.e., belonging to the CVT class). These findings suggest that the bilateral part of anterior prefrontal cortex and right posterior supramarginal gyrus helps in integrating neural activity across different brain areas via shortest paths to ensure effective communication with minimal delay [81]. Moreover, the findings related to the dorsolateral prefrontal cortex suggest that its engagement increases with increase in difficulty level of the task.

(c) **NB Analysis**: The results of the NB values as depicted by the radar plot in Fig. 11(c) portray the same BAs for each creative class label as indicated by the NE based evaluation. The high NB values for the specified BAs signify that they serve as key intermediaries in the flow of information between other brain lobes. In other words, high NB nodes act as bridges or hubs that connect different brain regions, ensuring efficient communication across the entire network [37].

Hence, the node based feature analysis discussed above supports the proposition that, for analogical reasoning, the BAs that act as prime controllers of the entire brain network include the bilateral anterior prefrontal cortex (BA 10 corresponding to nodes 1 and 8) and right posterior supramarginal gyrus (BA 40 corresponding to node 14). The observed findings are in agreement with prior research in [24], [25], [32], [72]. Additionally, the analysis reveals that the engagement of the bilateral region of dorsolateral prefrontal cortex (BA 46, corresponding to nodes 2 and 9) varies with the difficulty level of the problem, with higher activation indicating greater difficulty and vice versa [82], [83].

D. OPTIMIZATION OF CLASSIFIER PARAMETERS

Hyper-parameter optimization of the proposed EGCIFC model involves fine-tuning its parameters to ensure optimal performance in categorizing the target class labels. In the present context, the optimal settings for the hyper-parameters were determined using the random search algorithm [65]. The rationale for choosing this algorithm lies in its efficiency in exploring the search space with low computational time [65], [84]. The model's performance was assessed using the 10-fold cross-validation across different parameter configurations. In this method, the dataset for each subject was divided into 10 separate folds. For each parameter configuration, the model was trained using 9 folds and tested on the remaining fold. This process was repeated over 10 runs, with the test fold changing each time. As a result, the training and testing sets for each subject contained data from the same individual but remained distinct in each run. Random search was conducted for a total of 100 iterations. The classifier performance did not exhibit appreciable improvements beyond 60 iterations, indicating convergence. Therefore, only 60 iterations were considered for the classification task. Once the highest accuracy was achieved across all candidate settings, the best configuration was applied to the test set. The first hyper-parameter of EGCIFC involves the truncation of exp(A) till the third order, ensuring an optimal balance between computational efficiency and classification accuracy. The rest of the optimal hyper-parameter values of the model are: $Q = 2$, $L = 64$, $R = 32$, $\eta_1 = 19.27$, $\eta_2 = 34.96$, $\eta_3 = 56.11$, $\eta_4 = 81.23$.

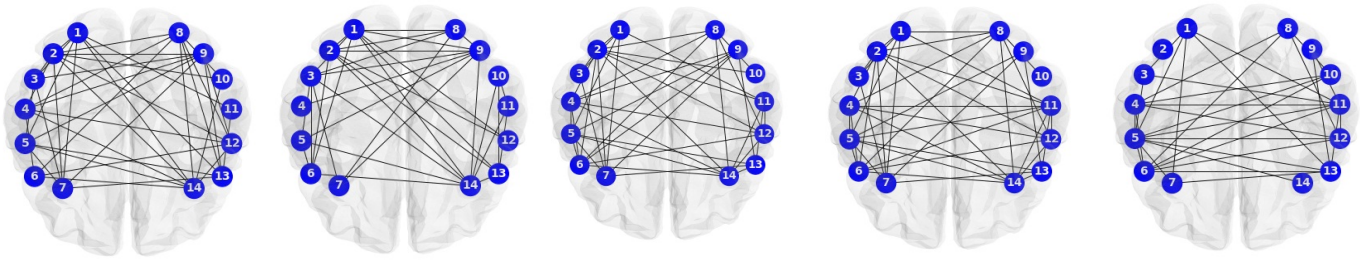

(a) (b) (c) (d) (e)

Fig. 10. The brain connectivity networks obtained for each class of subject in WBCDS: (a) subject ID: I27 who could correctly solve the RAPM task of very high difficulty level, (b) subject ID: I11 who could correctly solve the RAPM task of high difficulty level, (c) subject ID: I09 who could correctly solve the RAPM task of medium difficulty level, (d) subject ID: I32 who could correctly solve the RAPM task of easy level, and (e) subject ID: I05 who could not solve the RAPM task of any difficulty level.

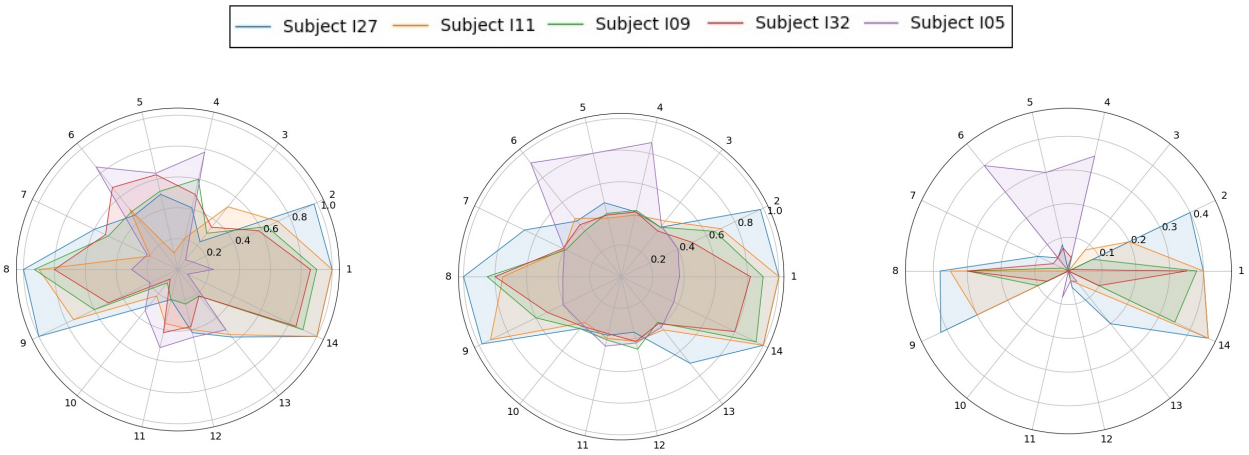

(a) (b) (c)

Fig. 11. The radar plots for analyzing node-based brain connectivity features: (a) radar plot for node strength pertaining to 5 classes of subjects, (b) radar plot for node efficiency pertaining to 5 classes of subjects, and (c) radar plot for node betweenness pertaining to 5 classes of subjects.

V. PERFORMANCE ANALYSIS AND STATISTICAL VALIDATION OF THE PROPOSED MODEL

This section analyzes the performance of the proposed classifier by conducting five main steps: i) a comparative study with respect to its competitors, ii) an ablation study to understand the potential of individual components, iii) an analysis of the effect of reducing the FOU on performance, iv) a comparative study to understand the impact of different brain connectivity formulations on performance, and v) statistical validation of the results. The detailed analysis is presented below.

A. PERFORMANCE ANALYSIS OF THE PROPOSED EGCIFC WITH RESPECT TO SOTA TECHNIQUES

The performance of the proposed EGCIFC is analyzed in three distinct phases. First, the performance of the proposed model is compared with respect to the SOTA techniques utilizing the metrics discussed in Section II for the WBCDS, and the results are portrayed in Table I. It is apparent from this table that the proposed classifier achieved a CA of 98.77%, representing an improvement of 2.25% over its nearest competitor and 22.72% over the lowest performing-baseline. Similarly, the F1-score improved to 98.61%, surpassing the nearest and worst SOTA methods by 2.27% and 22.13% respectively. Furthermore, the TPR is significantly higher, and the FPR is notably lower than those achieved by existing techniques, underscoring the robustness and reliability of the proposed approach. The low standard deviations across all four metrics (i.e., $\pm 0.72\%$ in CA, $\pm 0.83\%$ in F1-score, ± 0.011 in TPR and ± 0.021 in FPR) further highlight the model's robust performance. Additionally, the results in Table I demonstrate that the runtime complexity of the proposed classifier is 92.23 ms, representing a reduction in run-time by 7.46% and 54.7% with respect to its nearest and lowest-performing SOTA methods.

Second, the performance of the proposed classifier is evaluated across three datasets, i.e., WBCDS, SWICDS, and NICDS. The results of this comparative analysis are presented in Table II. It is evident from the table that the proposed model consistently achieves high precision in classifying the target class labels across all datasets. This analysis highlights the model's strong generalization capability across diverse data distributions.

Third, a confusion matrix analysis is conducted to further demonstrate the robustness of the proposed model. The confusion matrices for each dataset are presented in Fig. 12. The results indicate that the model consistently achieves high precision in classifying the desired class labels across all datasets.

TABLE I
COMPARATIVE STUDY OF PROPOSED CLASSIFIER PERFORMANCE FOR WBCDS WITH RESPECT TO SOTA METHODS (CA, F1, TPR, AND FPR ARE REPORTED AS MEAN ± STANDARD DEVIATION; RUN-TIME COMPLEXITY IS REPORTED AS A SINGLE VALUE).

Classifiers with optimal parameter settings	**CA (%)**	**F1 (%)**	**TPR**	**FPR**	**Run-time complexity (ms)**
DCNN [85]	76.05 ± 7.88	76.48 ± 7.51	0.76 ± 0.137	0.56 ± 0.088	203.45
Chebnet [86]	77.48 ± 7.12	77.90 ± 6.36	0.78 ± 0.124	0.52 ± 0.096	162.72
DGCN [87]	84.35 ± 6.33	83.70 ± 6.87	0.85 ± 0.127	0.23 ± 0.091	116.34
ASGCNN [88]	88.96 ± 5.49	88.55 ± 6.94	0.87 ± 0.102	0.12 ± 0.115	368.61
AEGCN [89]	93.03 ± 3.66	92.81 ± 4.02	0.92 ± 0.074	0.08 ± 0.086	238.25
CNN-AE with IT2FR-GWO [90]	95.27 ± 3.02	95.03 ± 2.56	0.95 ± 0.063	0.01 ± 0.058	130.70
GC-IT2FN [46]	96.52 ± 1.34	96.34 ± 1.96	0.96 ± 0.045	0.009 ± 0.050	99.67
Proposed EGCIFC	**98.77 ± 0.72**	**98.61 ± 0.83**	**0.98 ± 0.011**	**0.003 ± 0.021**	**92.23**

TABLE II
AVERAGE PERFORMANCE OF THE PROPOSED CLASSIFIER ACROSS THREE DATASETS

Classifier Metrics	**Datasets**			**Average Metric Value**
	WBCDS	**SWICDS**	**NICDS**	
CA (%)	98.77	98.42	98.84	98.68
F1 (%)	98.61	98.37	98.81	98.60
TPR	0.986	0.983	0.988	0.986
FPR	0.003	0.002	0.002	0.002

Although a very few misclassified instances were observed, the overall classification trend remained stable. Misclassifications (with error rate computed as 1-CA) primarily occurred between adjacent creativity classes, such as FCT (error rate = 0.0388) and MCT (error rate = 0.0278) in WBCDS, FCT (error rate = 0.0308) and MCT (error rate = 0.0338) in SWICDS, and SCT (error rate = 0.0149) and FCT (error rate = 0.0196) in NICDS, possibly due to overlapping cognitive and neural characteristics. Although these misclassifications exist, they are minimal and do not compromise the classifier's robustness; instead, they further reinforce its accuracy and generalizability across datasets.

B. ABLATION STUDY OF THE PROPOSED EGCIFC MODEL

An extensive ablation study has been performed on the proposed EGCIFC model to analyze the contribution of its individual components on overall classification performance. Such an analysis is undertaken by systematically removing specific modules from the original architecture of the EGCIFC and then examining the corresponding effects on the classification results. Table III demonstrates the results of the aforesaid study.

It is observed from Table III that moderate CA and F1-score values are obtained when IT2FS classifier is utilized independently as it can tackle uncertainty but cannot effectively deal with graph based data. Similarly, a comparable trend in CA and F1-score is observed when the traditional GCN is used without (w/o) Smish (i.e., the traditional Logish [91] function is used instead) and without 1D spatial convolution (i.e., mean-pooling is used instead). The aforesaid result occurs due to GCN's capability to process graph-structured data but inability to address uncertainty. However, a slight improvement in CA and F1-score is observed when Smish is employed, underscoring the effectiveness of the activation function. Furthermore, GCN with Smish and 1D spatial convolution shows better CA and F1-score compared to the previous classifier configurations. Notably, EGCN with 1D spatial convolution achieves a significant improvement over its counterparts, highlighting its importance. Additionally, the inclusion of Smish further enhances the performance of EGCN.

There is a considerable increase in classifier performance when the IT2FS module is integrated with the GCN. It is important to note that both Smish and 1D spatial convolution play a critical role in enhancing performance for the above classifier architecture. Moreover, EGCN combined with IT2FS further improves classifier performance, with the second-best combination being EGCN w/o Smish + 1D spatial convolution + IT2FS, due to the absence of the Smish function. The best results are obtained from the proposed combination, i.e., EGCN + Smish + 1D spatial convolution + IT2FS, highlighting the contribution of each module within the proposed approach.

C. IMPACT OF MODIFICATION IN FOU ON CLASSIFIER PERFORMANCE

The impact of FOU reduction using the proposed LMF formulation (as discussed in Section III) is compared against the traditional FOU design, which is derived by taking the union of 10 Type-1 MFs obtained over 10 experimental days. The results of the aforesaid comparison are portrayed in Table IV. It is apparent from this table that the proposed FOU reduction technique leads to a significant improvement in both CA and F1-score values compared to the conventional method.

D. COMPARATIVE STUDY OF DIFFERENT APPROACHES OF BRAIN CONNECTIVITY NETWORK FORMATION

A comparative study with respect to CA and F1-score is conducted to examine the impact of the proposed model's performance by utilizing different formulations of brain connectivity networks. The comparison includes several widely used methods for constructing brain networks from fNIRS signals, such as Phase Locking Value (PLV) [92], [93], Phase Lag Index (PLI) [94], Mutual Information (MI) [95], [96], and Pearson's Correlation (PC) [97], [98]. All connectivity metrics mentioned above were computed on the same fNIRS signals, which were pre-processed using a 6th-order Chebyshev band-pass filter and ICA. These pre-processing steps minimized

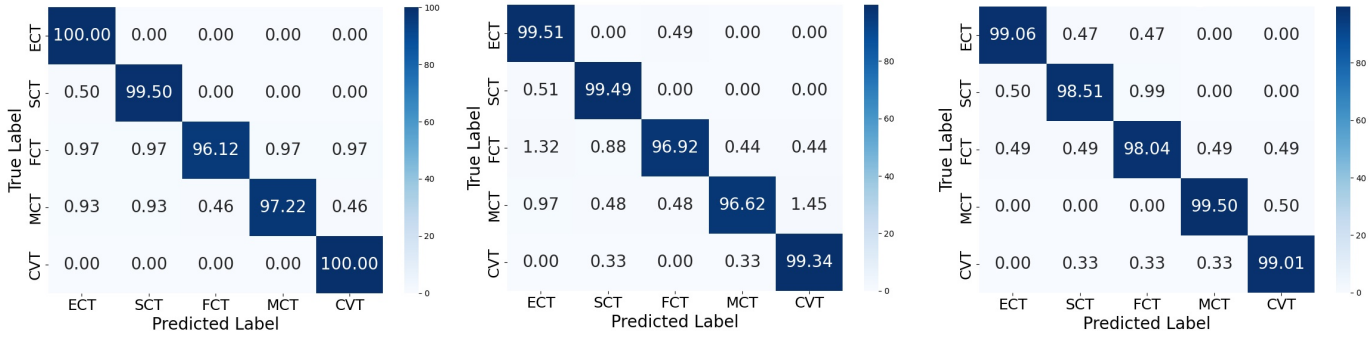

(a) (b) (c)

Fig. 12. The confusion matrix for three datasets (a) WBCDS (b) SWICDS (c) NICDS

TABLE III
ABLATION STUDY OF THE PROPOSED CLASSIFIER MODEL ACROSS THREE DATASETS

Variation in classifier modules	**Datasets**					
	WBCDS		**SWICDS**		**NICDS**	
	CA (%)	**F1 (%)**	**CA (%)**	**F1 (%)**	**CA (%)**	**F1 (%)**
IT2FS	87.95	87.34	88.20	88.65	87.69	87.62
GCN w/o Smish w/o 1D spatial convolution	88.97	88.72	89.02	88.84	88.36	88.21
GCN + Smish w/o 1D spatial convolution	89.46	89.32	89.66	89.61	89.54	89.50
GCN w/o Smish + 1D spatial convolution	89.85	89.72	89.78	89.71	89.96	89.88
GCN + Smish + 1D spatial convolution	89.97	90.02	90.21	90.18	90.11	90.03
EGCN w/o Smish w/o 1D spatial convolution	90.56	90.35	90.47	90.42	90.51	90.48
EGCN + Smish w/o 1D spatial convolution	90.78	90.70	90.81	90.86	90.94	90.90
EGCN w/o Smish + 1D spatial convolution	91.25	91.16	91.12	91.08	91.30	91.27
EGCN + Smish + 1D spatial convolution	91.73	91.68	91.45	91.52	91.92	91.86
GCN w/o Smish w/o 1D spatial convolution + IT2FS	93.54	93.61	93.03	93.11	93.43	93.37
GCN + Smish w/o 1D spatial convolution + IT2FS	93.72	93.68	93.27	93.30	93.62	93.55
GCN w/o Smish + 1D spatial convolution + IT2FS	94.56	94.63	94.40	94.51	94.60	94.57
GCN + Smish + 1D spatial convolution + IT2FS	94.80	94.77	94.64	94.66	94.85	94.81
EGCN w/o Smish w/o 1D spatial convolution + IT2FS	96.21	96.17	96.34	96.38	96.27	96.32
EGCN + Smish w/o 1D spatial convolution + IT2FS	96.60	96.52	96.68	96.71	96.76	96.81
EGCN w/o Smish + 1D spatial convolution + IT2FS	97.54	97.48	97.40	97.33	97.72	97.69
EGCN + Smish + 1D spatial convolution + IT2FS (i.e., EGCIFC)	**98.77**	**98.61**	**98.42**	**98.37**	**98.84**	**98.81**

TABLE IV
EFFECT OF RECTIFYING THE FOU ON CLASSIFIER PERFORMANCE

Dataset	**Modification in Classifier Architecture**			
	EGCIFC + original FOU		**EGCIFC + rectified FOU**	
	CA (%)	**F1 (%)**	**CA (%)**	**F1 (%)**
WBCDS	94.85	94.78	**98.77**	**98.61**
SWICDS	95.03	94.96	**98.42**	**98.37**
NICDS	95.56	95.43	**98.84**	**98.81**

TABLE V
IMPACT OF VARIOUS COMPUTATIONS OF BRAIN CONNECTIVITY NETWORKS ON CLASSIFIER PERFORMANCE

Brain network formulations	**Datasets**					
	WBCDS		**SWICDS**		**NICDS**	
	CA (%)	**F1 (%)**	**CA (%)**	**F1 (%)**	**CA (%)**	**F1 (%)**
PLV	93.27	93.23	93.54	93.50	93.72	93.76
PLI	93.20	93.18	93.56	93.61	94.02	93.94
MI	95.60	95.52	95.88	95.83	95.65	95.59
PC	97.11	97.06	96.78	96.72	97.01	96.97
WTC	**98.77**	**98.61**	**98.42**	**98.37**	**98.84**	**98.81**

the impact of physiological and motion artifacts, ensuring consistent and fair connectivity estimation across methods. A detailed description of the adaptation of the above metrics to fNIRS signals is provided in Section A.IV of the Appendix [55]. The results of the current comparative study, as shown in Table V, highlight a significant improvement in the performance of the proposed classifier with WTC based network construction in comparison to the traditional formulations.

E. STATISTICAL VALIDATION OF THE PROPOSED MODEL

The statistical validation of the proposed EGCIFC model has been carried out using the popular Friedman's non-parametric statistical test [99]. According to the Friedman test, the algorithm with the best performance is assigned the lowest rank. The Friedman static χ_F^2 corresponding to $(g-1)$ degrees of freedom is computed using (21).

$$\chi_F^2 = \frac{12D}{g(g+1)}\left[\sum_{v=1}^{g} R_v^2 - \frac{g(g+1)^2}{4}\right] \tag{21}$$

where, D signifies the number of datasets (here, 3), g depicts the number of classifier algorithms (here, 8), and R_v represents the average rank of the y^{th} algorithm to the z^{th} dataset. The results of the above statistical test is depicted by Table VI. It is apparent from this table that the Friedman's static χ_F^2=19.95

TABLE VI
FRIEDMAN'S TEST TO VALIDATE THE PROPOSED MODEL

Classifier Algorithms	R_v	χ_F^2
DCNN	7.83	**19.95 (Null Hypothesis Rejected)**
Chebnet	6.92	
DGCN	6.17	
ASGCNN	5	
AEGCN	3.75	
CNN-AE+IT2FR-GWO	3.25	
GC-IT2FN	2	
EGCIFC	**1**	

¿ $\chi^2_{7,0.95}$=14.07, which represents the chi-square value at 95% confidence level with 7 degrees of freedom. The statistical test results indicate that the null hypothesis, which posits that all classifier algorithms are equivalent in terms of performance, is rejected. Thus, it is crucial to conduct further analysis and comparison of the algorithms based on their respective ranks.

VI. CONCLUSION

Understanding the cognitive underpinnings of scientific creative skill in individuals is still an open-ended problem in neuroscience. The present study offers a valuable contribution to the above problem by leveraging fNIRS data to assess the levels of creative ability in subjects through brain connectivity analysis. The aforementioned analysis conducted using three node based connectivity features (strength, efficiency and betweeness) infers the active participation of bilateral anterior prefrontal cortex (BA 10) and right posterior supramarginal gyrus (BA 40) while solving the RAPM task. Additionally, the bilateral regions of dorsolateral prefrontal cortex (BA 46) become highly engaged whenever the difficulty level of the problems rises. Furthermore, the node based features are classified by a novel EGCIFC model that can efficiently identify different levels of subjective creative potential in comparison to SOTA methods.

Thus, the proposed scheme has the potential to be utilized as a recruitment strategy for placing individuals in various industrial departments based on their respective creative ability grades. For instance, an extremely creative thinker could be appointed as a research and development lead, a superbly creative thinker as an innovation manager, a medium-level/fairly creative thinker as a product design specialist, while a low-level/mildly creative thinker as a quality assurance analyst. This strategic placement would ensure optimal utilization of each individual's creative potential, fostering innovation and efficiency within industrial sectors.

A limitation of the proposed study lies in the analysis of brain responses within a fixed 15-second problem-solving window. This duration was experimentally validated, as all participants were able to complete the problems within 15 seconds, and additional time did not significantly improve their performance. However, the possibility that some individuals might succeed with more time cannot be entirely ruled out. Another limitation is that RAPM test primarily assesses analogical reasoning and does not capture other cognitive traits that contribute to scientific creativity, such as divergent thinking, deductive reasoning, and the like. Future work could focus on developing a unified framework to assess multiple cognitive dimensions of scientific creativity. Additionally, this study opens avenues for developing computational models of scientific creativity inspired by underlying biological mechanisms.

REFERENCES

[1] R. K. Sawyer and D. Henriksen, *Explaining creativity: The science of human innovation*. Oxford university press, 2024.

[2] A. Abraham, *The neuroscience of creativity*. Cambridge University Press, 2018.

[3] S. Ghosh, A. Konar, and A. K. Nagar, "Decoding subjective creativity skill from visuo-spatial reasoning ability using capsule graph neural network," in *2021 International Joint Conference on Neural Networks (IJCNN)*. IEEE, 2021, pp. 1–8.

[4] L. Ghosh, R. Kar, A. Konar, A. Chakraborty, and A. K. Nagar, "Identification of brain activation regions in inductive learning based scientific creativity test," in *2018 IEEE Symposium Series on Computational Intelligence (SSCI)*. IEEE, 2018, pp. 950–957.

[5] S. Ghosh and A. Konar, "Decoding the scientific creative-ability of subjects using dual attention induced graph convolutional-capsule network," *Applied Soft Computing*, vol. 161, p. 111769, 2024.

[6] J. C. Kaufman and R. J. Sternberg, *The Cambridge Handbook of Creativity*. Cambridge University Press, 2019.

[7] H. B. de Vries and T. I. Lubart, "Scientific creativity: divergent and convergent thinking and the impact of culture," *The Journal of Creative Behavior*, vol. 53, no. 2, pp. 145–155, 2019.

[8] R. W. Weisberg, *Analogical Thinking in Problem-Solving and Creativity*. Cambridge University Press, 2020, p. 145–180.

[9] S. I. Robertson, *Problem solving: Perspectives from cognition and neuroscience*. Psychology Press, 2016.

[10] R. Bianchi and I. S. Schonfeld, "Occupational depression, cognitive performance, and task appreciation: A study based on raven's advanced progressive matrices," *Frontiers in psychology*, vol. 12, p. 695539, 2021.

[11] L. Cipolotti, J. K. Ruffle, J. Mole, T. Xu, H. Hyare, T. Shallice, E. Chan, and P. Nachev, "Graph lesion-deficit mapping of fluid intelligence," *Brain*, vol. 146, no. 1, pp. 167–181, 2023.

[12] D. F. Lohman and J. M. Lakin, "Intelligence and reasoning," *The Cambridge handbook of intelligence*, pp. 419–441, 2011.

[13] K. McGreggor, M. Kunda, and A. K. Goel, "A fractal approach towards visual analogy." in *ICCC*, 2010, pp. 65–74.

[14] M. Ragni and S. Neubert, "Solving raven's iq-tests: an ai and cognitive modeling approach," in *ECAI 2012*. IOS Press, 2012, pp. 666–671.

[15] C. Díaz-Rodríguez and E. Pérez-Córdoba, "Influence of problem-solving ability and personality variables on the improvement and creativity of tactical decisions in basketball," *Frontiers in Psychology*, vol. 15, p. 1450084, 2024.

[16] K. McGreggor, M. Kunda, and A. Goel, "Fractals and ravens," *Artificial Intelligence*, vol. 215, pp. 1–23, 2014.

[17] D. A. Joyner, D. Bedwell, C. Graham, W. Lemmon, O. Martinez, and A. K. Goel, "Using human computation to acquire novel methods for addressing visual analogy problems on intelligence tests." in *ICCC*, 2015, pp. 23–30.

[18] S. W. Kwon, "Differences in neural current sources of science gifted and normal children in creative reasoning," *Journal of Korean Elementary Science Education*, vol. 34, no. 1, pp. 131–141, 2015.

[19] K. McGreggor, M. Kunda, and A. K. Goel, "Fractal analogies: Preliminary results from the raven's test of intelligence." in *ICCC*, 2011, pp. 69–71.

[20] Y. Liu, K. He, K. Man, and P. Zhan, "Exploring critical eye-tracking metrics for identifying cognitive strategies in raven's advanced progressive matrices: A data-driven perspective," *Journal of Intelligence*, vol. 13, no. 2, p. 14, 2025.

[21] A. Chuderski, J. Jastrzebski, B. Kroczek, H. Kucwaj, and M. Ociepka, "Metacognitive experience on raven's matrices versus insight problems," *Metacognition and Learning*, vol. 16, pp. 15–35, 2021.

[22] N. Friedman, T. Fekete, K. Gal, and O. Shriki, "Eeg-based prediction of cognitive load in intelligence tests," *Frontiers in human neuroscience*, vol. 13, p. 191, 2019.

[23] T. Xu, J. Wang, G. Zhang, L. Zhang, and Y. Zhou, "Confused or not: decoding brain activity and recognizing confusion in reasoning learning using eeg," *Journal of Neural Engineering*, vol. 20, no. 2, p. 026018, 2023.

[24] T. M. Morin, K. N. Moore, K. Isenburg, W. Ma, and C. E. Stern, "Functional reconfiguration of task-active frontoparietal control network facilitates abstract reasoning," *Cerebral Cortex*, vol. 33, no. 10, pp. 5761–5773, 2023.

[25] L. Anat, R. Reut, I. Nofar, T. Niv, S. Maayan, T. Galia, and L. Abigail, "The role of the cerebellum in fluid intelligence: An fmri study," *Cognitive Systems Research*, vol. 83, p. 101178, 2024.

[26] Z. Chen, A. De Beuckelaer, X. Wang, and J. Liu, "Distinct neural substrates of visuospatial and verbal-analytic reasoning as assessed by raven's advanced progressive matrices," *Scientific reports*, vol. 7, no. 1, p. 16230, 2017.

[27] H. U. Amin, A. S. Malik, M. Hussain, N. Kamel, and W.-T. Chooi, "Brain behavior during reasoning and problem solving task: an eeg study," in *2014 5th International Conference on Intelligent and Advanced Systems (ICIAS)*. IEEE, 2014, pp. 1–4.

[28] S. Jawed, H. U. Amin, A. S. Malik, and I. Faye, "Hemispheric asymmetries in electroencephalogram oscillations for long-term memory retrieval in healthy individuals," *Brain Sciences*, vol. 10, no. 12, p. 937, 2020.

[29] M. Ociepka, P. Kałamała, and A. Chuderski, "Take your time: Slow brain rhythms predict fluid intelligence," *Intelligence*, vol. 100, p. 101780, 2023.

[30] W. Luo and R. Zhou, "Can working memory task-related eeg biomarkers measure fluid intelligence and predict academic achievement in healthy children?" *Frontiers in Behavioral Neuroscience*, vol. 14, p. 2, 2020.

[31] H. U. Amin, A. S. Malik, N. Kamel, W.-T. Chooi, and M. Hussain, "P300 correlates with learning & memory abilities and fluid intelligence," *Journal of neuroengineering and rehabilitation*, vol. 12, pp. 1–14, 2015.

[32] S. Ghosh, A. Konar, and A. K. Nagar, "Analyzing the creative potential of subjects using eeg-induced capsule graph neural network," in *2024 International Joint Conference on Neural Networks (IJCNN)*. IEEE, 2024, pp. 1–8.

[33] N. Babu, U. Satija, J. Mathew, and A. Vinod, "Emotion recognition in virtual and non-virtual environments using eeg signals: Dataset and evaluation," *Biomedical Signal Processing and Control*, vol. 106, p. 107674, 2025.

[34] Y. Zhang, J. Qu, Q. Zhang, and C. Cheng, "Eeg-based emotion recognition based on 4d feature representations and multiple attention mechanisms," *Biomedical Signal Processing and Control*, vol. 103, p. 107432, 2025.

[35] C. Brunner, M. Billinger, M. Seeber, T. R. Mullen, and S. Makeig, "Volume conduction influences scalp-based connectivity estimates," *Frontiers in computational neuroscience*, vol. 10, p. 121, 2016.

[36] J. Park, J. Shin, and J. Jeong, "Inter-brain synchrony levels according to task execution modes and difficulty levels: an fnirs/gsr study," *IEEE Transactions on Neural Systems and Rehabilitation Engineering*, vol. 30, pp. 194–204, 2022.

[37] A. Fornito, A. Zalesky, and E. Bullmore, *Fundamentals of brain network analysis*. Academic press, 2016.

[38] T. N. Kipf and M. Welling, "Semi-supervised classification with graph convolutional networks," *arXiv preprint arXiv:1609.02907*, 2016.

[39] K. Qin, D. Lei, W. H. Pinaya, N. Pan, W. Li, Z. Zhu, J. A. Sweeney, A. Mechelli, and Q. Gong, "Using graph convolutional network to characterize individuals with major depressive disorder across multiple imaging sites," *EBioMedicine*, vol. 78, 2022.

[40] S. Zhang, H. Tong, J. Xu, and R. Maciejewski, "Graph convolutional networks: a comprehensive review," *Computational Social Networks*, vol. 6, no. 1, pp. 1–23, 2019.

[41] Z. Wu, S. Pan, F. Chen, G. Long, C. Zhang, and P. S. Yu, "A comprehensive survey on graph neural networks," *IEEE transactions on neural networks and learning systems*, vol. 32, no. 1, pp. 4–24, 2020.

[42] S. Anwer, H. Li, M. F. Antwi-Afari, A. M. Mirza, M. A. Rahman, I. Mehmood, R. Guo, and A. Y. L. Wong, "Evaluation of data processing and artifact removal approaches used for physiological signals captured using wearable sensing devices during construction tasks," *Journal of Construction Engineering and Management*, vol. 150, no. 1, p. 03123008, 2024.

[43] R. Huang, K.-S. Hong, D. Yang, and G. Huang, "Motion artifacts removal and evaluation techniques for functional near-infrared spectroscopy signals: a review," *Frontiers in Neuroscience*, vol. 16, p. 878750, 2022.

[44] M. Laha, A. Konar, P. Rakshit, and A. K. Nagar, "Hemodynamic analysis for olfactory perceptual degradation assessment using generalized type-2 fuzzy regression," *IEEE Transactions on Cognitive and Developmental Systems*, vol. 14, no. 3, pp. 1217–1231, 2021.

[45] M. Laha, A. Konar, and A. K. Nagar, "Olfactory perceptual-ability assessment by near-infrared spectroscopy using vertical-slice based fuzzy reasoning," *IEEE Access*, vol. 11, pp. 17 779–17 792, 2023.

[46] S. Ghosh, A. Konar, and A. K. Nagar, "Cognitive assessment of scientific creative-skill by brain-connectivity analysis using graph convolutional-interval type-2 fuzzy network," *IEEE Transactions on Cognitive and Developmental Systems*, 2024.

[47] X. Wang, H. Ren, and A. Wang, "Smish: A novel activation function for deep learning methods," *Electronics*, vol. 11, no. 4, p. 540, 2022.

[48] D. Wu, "On the fundamental differences between interval type-2 and type-1 fuzzy logic controllers," *IEEE Transactions on Fuzzy Systems*, vol. 20, no. 5, pp. 832–848, 2012.

[49] Y. Zhang, H. Ishibuchi, and S. Wang, "Deep takagi–sugeno–kang fuzzy classifier with shared linguistic fuzzy rules," *IEEE Transactions on Fuzzy Systems*, vol. 26, no. 3, pp. 1535–1549, 2017.

[50] R. Zurrin, S. T. S. Wong, M. M. Roes, C. M. Percival, A. Chinchani, L. Arreaza, M. Kusi, A. Momeni, M. Rasheed, Z. Mo *et al.*, "Functional brain networks involved in the raven's standard progressive matrices task and their relation to theories of fluid intelligence," *Intelligence*, vol. 103, p. 101807, 2024.

[51] A. E. Green, D. J. Kraemer, J. A. Fugelsang, J. R. Gray, and K. N. Dunbar, "Neural correlates of creativity in analogical reasoning." *Journal of Experimental Psychology: Learning, Memory, and Cognition*, vol. 38, no. 2, p. 264, 2012.

[52] A. E. Green, "Creativity, within reason: Semantic distance and dynamic state creativity in relational thinking and reasoning," *Current Directions in Psychological Science*, vol. 25, no. 1, pp. 28–35, 2016.

[53] C.-Y. Kao, "How figurativity of analogy affects creativity: The application of four-term analogies to teaching for creativity," *Thinking skills and creativity*, vol. 36, p. 100653, 2020.

[54] M. S. Vendetti, A. Wu, and K. J. Holyoak, "Far-out thinking: Generating solutions to distant analogies promotes relational thinking," *Psychological science*, vol. 25, no. 4, pp. 928–933, 2014.

[55] "Appendix: Attached as a supplementary file in the submission portal."

[56] N. Naseer and K.-S. Hong, "fnirs-based brain-computer interfaces: a review," *Frontiers in human neuroscience*, vol. 9, p. 3, 2015.

[57] H. Wang, X. Zhang, J. Li, B. Li, X. Gao, Z. Hao, J. Fu, Z. Zhou, and M. Atia, "Driving risk cognition of passengers in highly automated driving based on the prefrontal cortex activity via fnirs," *Scientific Reports*, vol. 13, no. 1, p. 15839, 2023.

[58] V. Kumar, M. Arya, A. Kumar, and D. K. Jhariya, "Design and comparison between iir butterworth and chebyshev digital filters using matlab," in *2024 Fourth International Conference on Advances in Electrical, Computing, Communication and Sustainable Technologies (ICAECT)*. IEEE, 2024, pp. 1–7.

[59] E. Oja and Z. Yuan, "The fastica algorithm revisited: Convergence analysis," *IEEE transactions on Neural Networks*, vol. 17, no. 6, pp. 1370–1381, 2006.

[60] N. Selvaraj, Y. Mendelson, K. H. Shelley, D. G. Silverman, and K. H. Chon, "Statistical approach for the detection of motion/noise artifacts in photoplethysmogram," in *2011 Annual International Conference of the IEEE Engineering in Medicine and Biology Society*. IEEE, 2011, pp. 4972–4975.

[61] A. Aarabi and T. J. Huppert, "Characterization of the relative contributions from systemic physiological noise to whole-brain resting-state functional near-infrared spectroscopy data using single-channel independent component analysis," *Neurophotonics*, vol. 3, no. 2, pp. 025 004–025 004, 2016.

[62] A. Grinsted, J. C. Moore, and S. Jevrejeva, "Application of the cross wavelet transform and wavelet coherence to geophysical time series," *Nonlinear processes in geophysics*, vol. 11, no. 5/6, pp. 561–566, 2004.

[63] H. Zaynidinov, U. Juraev, S. Tishlikov, and J. Modullayev, "Application of daubechies wavelets in digital processing of biomedical signals and images," in *International Conference on Intelligent Human Computer Interaction*. Springer, 2023, pp. 194–206.

[64] B. C. Van Wijk, C. J. Stam, and A. Daffertshofer, "Comparing brain networks of different size and connectivity density using graph theory," *PloS one*, vol. 5, no. 10, p. e13701, 2010.

[65] J. Bergstra and Y. Bengio, "Random search for hyper-parameter optimization," *The journal of machine learning research*, vol. 13, no. 1, pp. 281–305, 2012.

[66] A. Khasnobish, A. Konar, D. N. Tibarewala, and A. K. Nagar, "Bypassing the natural visual-motor pathway to execute complex movement related tasks using interval type-2 fuzzy sets," *IEEE Transactions on Neural Systems and Rehabilitation Engineering*, vol. 25, no. 1, pp. 91–105, 2016.

[67] A. Konar, *Computational Intelligence: Principles, techniques and applications*. Springer Science & Business Media, 2006.
[68] M. Laha, A. Konar, P. Rakshit, L. Ghosh, S. Chaki, A. L. Ralescu, and A. K. Nagar, "Hemodynamic response analysis for mind-driven typewriting using a type 2 fuzzy classifier," in *2018 IEEE international conference on fuzzy systems (FUZZ-IEEE)*. IEEE, 2018, pp. 1–8.
[69] R. Navarro-Almanza, M. A. Sanchez, G. Licea, and J. R. Castro, "Knowledge transfer for labeling unknown fuzzy sets using grammar-guided genetic algorithms," *Applied Soft Computing*, vol. 124, p. 109019, 2022.
[70] S. Singh and S. Lalotra, "On generalized correlation coefficients of the hesitant fuzzy sets with their application to clustering analysis," *Computational and Applied Mathematics*, vol. 38, no. 1, p. 11, 2019.
[71] J.-S. R. Jang, C.-T. Sun, and E. Mizutani, "Neuro-fuzzy and soft computing-a computational approach to learning and machine intelligence [book review]," *IEEE Transactions on automatic control*, vol. 42, no. 10, pp. 1482–1484, 1997.
[72] J. Duncan, M. Assem, and S. Shashidhara, "Integrated intelligence from distributed brain activity," *Trends in cognitive sciences*, vol. 24, no. 10, pp. 838–852, 2020.
[73] F. Faul, E. Erdfelder, A.-G. Lang, and A. Buchner, "G* power 3: A flexible statistical power analysis program for the social, behavioral, and biomedical sciences," *Behavior research methods*, vol. 39, no. 2, pp. 175–191, 2007.
[74] "The database wbcds is uploaded in the google drive," 2025. [Online]. Available: https://drive.google.com/file/d/1gVXlkzLJl8cMLlcb4-dw9mH8DMZ81OQA/view?usp=sharing
[75] "The database swicds is uploaded in the google drive," 2025. [Online]. Available: https://drive.google.com/file/d/1hKOn56Spz9ZhRDpnw_9IE8HDVTIP1wkX/view?usp=sharing
[76] "The database nicds is uploaded in the google drive," 2025. [Online]. Available: https://drive.google.com/file/d/1Bd1z5o8OJ-1vsvcDY5nqlVEe4ER72Vy-/view?usp=sharing
[77] S. Xu, M. J. Reiss, and W. Lodge, "Comprehensive scientific creativity assessment (c-sca): A new approach for measuring scientific creativity in secondary school students," *International Journal of Science and Mathematics Education*, vol. 23, no. 2, pp. 293–319, 2025.
[78] W. Aschauer, K. Haim, and C. Weber, "A contribution to scientific creativity: A validation study measuring divergent problem solving ability," *Creativity Research Journal*, vol. 34, no. 2, pp. 195–212, 2022.
[79] G. A. of the World Medical Association *et al.*, "World medical association declaration of helsinki: ethical principles for medical research involving human subjects," *The Journal of the American College of Dentists*, vol. 81, no. 3, pp. 14–18, 2014.
[80] "The ethics committee report is uploaded in the google drive," 2025. [Online]. Available: https://drive.google.com/file/d/12nKOUNfE_nXKzxiUlCOHBxr5qwXREKp3/view?usp=sharing
[81] M. L. Stanley, M. N. Moussa, B. M. Paolini, R. G. Lyday, J. H. Burdette, and P. J. Laurienti, "Defining nodes in complex brain networks," *Frontiers in computational neuroscience*, vol. 7, p. 169, 2013.
[82] J. Molina del Río, M. A. Guevara, M. Hernández González, R. M. Hidalgo Aguirre, and M. A. Cruz Aguilar, "Eeg correlation during the solving of simple and complex logical–mathematical problems," *Cognitive, Affective, & Behavioral Neuroscience*, vol. 19, pp. 1036–1046, 2019.
[83] E. Juliyanto, P. Marwoto, R. Iswari, S. Nugroho, B. Mindyarto *et al.*, "Brain activity of problem solving proccess: a systematic literarure review," in *Journal of Physics: Conference Series*, vol. 1918, no. 5. IOP Publishing, 2021, p. 052068.
[84] L. Yang and A. Shami, "On hyperparameter optimization of machine learning algorithms: Theory and practice," *Neurocomputing*, vol. 415, pp. 295–316, 2020.
[85] J. Atwood and D. Towsley, "Diffusion-convolutional neural networks," *Advances in neural information processing systems*, vol. 29, 2016.
[86] M. Defferrard, X. Bresson, and P. Vandergheynst, "Convolutional neural networks on graphs with fast localized spectral filtering," *Advances in neural information processing systems*, vol. 29, 2016.
[87] C. Zhuang and Q. Ma, "Dual graph convolutional networks for graph-based semi-supervised classification," in *Proceedings of the 2018 world wide web conference*, 2018, pp. 499–508.
[88] H. Chang, B. Liu, Y. Zong, C. Lu, and X. Wang, "Eeg-based parkinson's disease recognition via attention-based sparse graph convolutional neural network," *IEEE Journal of Biomedical and Health Informatics*, vol. 27, no. 11, pp. 5216–5224, 2023.
[89] M. Ma, S. Na, and H. Wang, "Aegcn: An autoencoder-constrained graph convolutional network," *Neurocomputing*, vol. 432, pp. 21–31, 2021.
[90] A. Shoeibi, N. Ghassemi, M. Khodatars, P. Moridian, A. Khosravi, A. Zare, J. M. Gorriz, A. H. Chale-Chale, A. Khadem, and U. Rajendra Acharya, "Automatic diagnosis of schizophrenia and attention deficit hyperactivity disorder in rs-fmri modality using convolutional autoencoder model and interval type-2 fuzzy regression," *Cognitive neurodynamics*, vol. 17, no. 6, pp. 1501–1523, 2023.
[91] H. Zhu, H. Zeng, J. Liu, and X. Zhang, "Logish: A new nonlinear nonmonotonic activation function for convolutional neural network," *Neurocomputing*, vol. 458, pp. 490–499, 2021.
[92] P. Xie, Z. Nie, T. Zhang, G. Xu, A. Sun, T. Chen, and Y. Lv, "Fnirs based study of brain network characteristics in children with cerebral palsy during bilateral lower limb movement," *Medical Physics*, vol. 51, no. 6, pp. 4434–4446, 2024.
[93] S. I. Alzahrani, "Decoding contralateral finger movements from fnirs signals using phase connectivity features," in *2024 International Conference on Engineering and Emerging Technologies (ICEET)*. IEEE, 2024, pp. 1–6.
[94] J. Lu, J. Wang, Y. Cheng, Z. Shu, Y. Wang, X. Zhang, Z. Zhu, Y. Yu, J. Wu, J. Han *et al.*, "A knowledge-driven framework discovers brain activation-transition-spectrum (acts) features for parkinson's disease," *IEEE Transactions on Neural Systems and Rehabilitation Engineering*, 2024.
[95] M. U. Dalmış and A. Akın, "Similarity analysis of functional connectivity with functional near-infrared spectroscopy," *Journal of Biomedical Optics*, vol. 20, no. 8, p. 086012, 2015.
[96] M. Dadgostar, Z. Einalou, S. Setarehdam, H. Keskin-Ergen, and A. Akin, "Comparison of mutual information and partial correlation for functional connectivity in fnirs," in *Proceedings of the 21th Iranian Conference on Electric Engineering, Mashhad, Iran*, 2013, pp. 14–16.
[97] T. Nguyen, M. Kim, J. Gwak, J. J. Lee, K. Y. Choi, K. H. Lee, and J. G. Kim, "Investigation of brain functional connectivity in patients with mild cognitive impairment: a functional near-infrared spectroscopy (fnirs) study," *Journal of Biophotonics*, vol. 12, no. 9, p. e201800298, 2019.
[98] M. A. Yaqub, S.-W. Woo, and K.-S. Hong, "Effects of hd-tdcs on resting-state functional connectivity in the prefrontal cortex: An fnirs study," *Complexity*, vol. 2018, no. 1, p. 1613402, 2018.
[99] J. Demšar, "Statistical comparisons of classifiers over multiple data sets," *Journal of Machine learning research*, vol. 7, no. Jan, pp. 1–30, 2006.

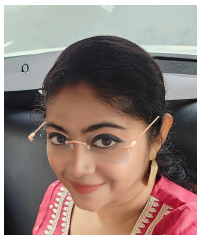

SAYANTANI GHOSH received her B.Tech. degree in Electronics and Communication Engineering from Dr. Sudhir Chandra Sur Degree Engineering College, Kolkata, India in 2015, and her M. Tech. degree in Intelligent Automation and Robotics (IAR) from the department of Electronics and Tele-Communication Engineering, Jadavpur University, Kolkata in 2018. She is currently working towards the Ph.D. degree in Artificial Intelligence and Cognitive Neuroscience from Jadavpur University under the guidance of Prof. Amit Konar. She is the recepient of 'Jodh Ishwar Singh (JIS) Sanman for Academic Excellence' by JIS Group, West Bengal, India in 2015, IEEE Brain Best Paper Award Runner Up by IEEE Symposium Series on Computational Intelligence (SSCI), Florida, USA in 2021 and IEEE Best Paper Award in the track Signal Processing and Computing Systems by International Conference on Computers and Devices for Communication (CODEC), Kolkata, India, in 2023. Her current research interests include Computational Creativity, Deep Learning, Brain-Computer Interfaces, Biological Underpinning of Perception and Scientific Creativity. She serves as a reviewer for IEEE Transactions on Emerging Topics in Computaional Intelligence, IEEE Transactions on Neural Systems and Rehabilitation Engineering, IEEE Transactions on Fuzzy Systems, IEEE Transactions on Artificial Intelligence and Knowledge Based Systems.

AMIT KONAR (SM' 2010) is currently a Professor in the department of Electronics and Tele-Communication Engineering, Jadavpur University, Kolkata, India. He earned his B.E. degree in Electronics and Tele-Communication Engineering from Indian Institute of Engineering Science and Technology (previously, Bengal Engineering College), Kolkata in 1983, his M.E. degree in Control Engineering, M. Phil. degree in System Modelling and Ph.D. degree in Artificial Intelligence, all from Jadavpur University in 1985, 1988 and 1994 respectively.

Dr. Konar is the author of 15 books including two popular texts, Artificial Intelligence and Soft Computing: Behavioral and Cognitive Modeling of the Human Brain, (CRC Press) in 2000 and Computational Intelligence: Principles, Techniques and Applications, (Springer) in 2005. He has published 35 peer-reviewed book chapters and over 100 research papers in leading international journals (including 30 IEEE Transactions), and over 250 research papers published in IEEE Flagship Conference proceeedings. He has supervised 29 Ph.D. theses and over 400 Masters theses, all in the broad area of Cognitive Neuro-science, AI and Robotics. Dr. Konar delivered keynote/tutorial speech in top flagship IEEE Conferences including WCCI-2020 and ICASSP-2016. He has been serving as the Associate Editor of IEEE TFS and IEEE TETCI for several years. Dr. Konar is currently the EIC of the Springer book series on Cognitive Intelligence and Robotics. He served as the Coordinator/Principal Investigator of several National level projects funded by Government of india and industries. His current research interest includes Cognitive Neuroscience, Type-2 Fuzzy Logic, Multi-agent Systems and Scientific Creativity.

ATULYA K. NAGAR received his B.Sc. (Hons.), M.Sc., and M.Phil. (Hons. with distinction) degrees in Mathematical Physics from MDS University, Ajmer, India. He was awarded a prestigious Commonwealth Fellowship to pursue his D.Phil. in Applied Nonlinear Mathematics at the University of York, UK, which he completed in 1996. He currently serves as Professor of Mathematics and Pro Vice-Chancellor (Research) at Liverpool Hope University (LHU), UK. In this role, he leads the development of science and engineering across the university. He has previously served as the Head of the School of Mathematics, Computer Science, and Engineering - which he established bottom up - and as the Founding Dean of the Faculty of Science. An internationally recognised scholar with expertise at the intersection of nonlinear mathematics, theoretical computer science, and systems engineering, Prof. Nagar has authored over 550 publications in leading academic venues. He has edited volumes on intelligent systems/AI and applied mathematics, and has extensive experience in academic leadership in both the UK and India. His contributions to research evaluation and funding policy include serving as an expert reviewer for the BBSRC (Bioinformatics Panel), EPSRC (High-Performance Computing Panel), and as a member of the AHRC Peer Review College. He holds visiting professorships at premier Indian institutions such as IIT Roorkee, South Asian University, and the University of Madras, where he was appointed to the Sir C.V. Raman Chair, supported by the endowment named after Nobel Laureate C.V. Raman. Prof. Nagar also contributes to national research strategy and governance as a member of the JISC Research Strategy Group (UK), the UKRI Talent Panel College, the REF 2029 People, Culture, and Environment (PCE) Pilot Panel, and EPSRC's Impact Accelerator Panel. He is a Fellow of the Institute of Mathematics and Its Applications (FIMA) and the Higher Education Academy (FHEA). ORCID: https://orcid.org/0000-0001-5549-6435